

Comprehensive Performance Evaluation of YOLOv10, YOLOv9 and YOLOv8 on Detecting and Counting Fruitlet in Complex Orchard Environments

Ranjan Sapkota^{a,1}, Zhichao Meng^{b,1}, Dawood Ahmed^a, Martin Churuvija^a, Xiaoqiang Du^b,
Zenghong Ma^b, Manoj Karkee^{a*}

^aCenter for Precision & Automated Agricultural Systems, Washington State University, 24106 N Bunn Rd, Prosser, 99350, Washington, USA
^bSchool of Mechanical Engineering, Zhejiang Sci-Tech University, Hangzhou 310018, China

Abstract

Object detection, specifically fruitlet detection, is a crucial image processing technique in agricultural automation, enabling the accurate identification of fruitlets on orchard trees within images. It is vital for early fruit load management and overall crop management, facilitating the effective deployment of automation and robotics to optimize orchard productivity and resource use. This study systematically performed an extensive evaluation of the performances of all configurations of YOLOv8, YOLOv9, and YOLOv10 object detection algorithms in terms of precision, recall, mean Average Precision at 50% Intersection over Union (mAP@50), and computational speeds including pre-processing, inference, and post-processing times for fruitlet (of fruitlet) detection in commercial orchards. Additionally, this research performed and validated in-field counting of fruitlets using an iPhone and machine vision sensors in 5 different apple varieties (Scifresh, Scilate, Honeycrisp, Cosmic crisp & Golden delicious). This investigation of total 17 different configurations of YOLOv8, YOLOv9 and YOLOv10 (5 for YOLOv8, 6 for YOLOv9 and 6 for YOLOv10) revealed that YOLOv9 outperforms YOLOv10 and YOLOv8 in terms of mAP@50, while YOLOv10x outperformed all 17 configurations tested in terms of precision and recall. Specifically, YOLOv9 Gelan-e achieved the highest mAP@50 of 0.935, outperforming YOLOv10n's 0.921 and YOLOv8s's 0.924. In terms of precision, YOLOv10x achieved the highest precision of 0.908, indicating superior object identification accuracy compared to other configurations tested (e.g. YOLOv9 Gelan-c with a precision of 0.903 and YOLOv8m with 0.897). In terms of recall, YOLOv10s achieved the highest in its series (0.872), while YOLOv9 Gelan-m performed the best among YOLOv9 configurations (0.899), and YOLOv8n performed the best among the YOLOv8 configurations (0.883). Meanwhile, three configurations of YOLOv10; YOLOv10b, YOLOv10l, and YOLOv10x; outperformed all other configurations in YOLOv9 and YOLOv8 family of models in terms of post processing speed (only 1.5 ms), while YOLOv9 Gelan-e (1.9 ms) and YOLOv8m (2.1 ms). Furthermore, YOLOv8n exhibited the highest inference speed (detection speed) among all configurations tested, achieving a processing time of 4.1 milliseconds. In comparison, YOLOv9 Gelan-t and YOLOv10n also demonstrated impressive inference speeds of 9.3 ms and 5.5 ms, respectively. Additionally, counting validation studies across four apple varieties (Scifresh, Scilate, Honeycrisp, and Cosmic Crisp) using an iPhone 14, and two varieties (Golden Delicious and Scifresh) using Microsoft Kinect Azure DK and Intel RealSense D435i sensors, highlighted YOLOv9 Gelan-e as the most accurate configuration. It achieved an RMSE of 3.11 and an MAE of 4.58, surpassing all other YOLOv8, YOLOv9, and YOLOv10 configurations in accuracy. This performance underscores the YOLOv9 models' superiority in fruitlet detection and counting within complex orchard settings. Despite some YOLOv10 configurations offering marginally better precision and recall, the YOLOv9 models provide comparable accuracy while maintaining significantly faster inference speeds, making them more suited for agricultural applications where computational resources and data availability are often constrained.

Keywords: Fruitlet detection; You Only Look Once, YOLOv10, YOLOv9, YOLOv8, Precision Agriculture, Agricultural Automation, Robotics, Artificial Intelligence, YOLO

1. Introduction

Object detection in commercial orchards is the foundation to developing agricultural automation and robotics solutions for labor intensive tasks such as harvesting, thinning, and pruning [1], [2], [3]. One such labor-intensive operation in apple orchards is thinning green fruit in their early growth stage (fruitlets), which is crucial due to its role in enhancing crop yield and quality. Automating fruitlet thinning process is essential for minimizing the dependence

¹ These authors contributed equally to this work and should be considered co-first authors.

* Corresponding author

of rapidly depleting farm labor, which requires a robust machine vision system for fruitlet detection and localization in orchard environments [4], [5].

Most of the tree fruit crops often set a greater number of fruits per tree than the desired number which causes fruit-to-fruit competition for water, sunlight, and nutrients, resulting inadequate exposure of the fruits to the sun, less space to grow, and overall reduced fruit quality [4]. Additionally, too many fruits can result in reduced cold hardiness, breakage of tree limbs, and exhaustion of tree reserves [6]. Fruitlet thinning in the commercial production of tree fruit crops such as apples, kiwifruit, pears, peaches and plums has been practiced for thousands of years [7] to address these challenges and ensure optimal fruit size and quality [8] [9].

Apples is the third most consumed fruit in the United States (U.S.). U.S. also produces an average of 4.6 million tons of apples yearly, making the country the world's second-largest contributor in apple production. Around 382 thousand acres of land in the U.S. is used for farming apples commercially, which contributes to exporting 42 million bushels of apples worldwide with an estimated downstream value of \$21 billion dollars each year [10]. In the U.S., approximately 1.5 million hired workers are employed in agriculture annually, with about three-fourths or 1.1 million working in crop-production activities [11]. One of the most labor-intensive operations in apple production is fruitlet thinning, and therefore developing robotic fruitlet thinning solutions is essential for sustainable apple production in U.S and around the world [5], [12].

The availability of farm labor has continued to decline over the past decade, a situation worsened by the global pandemic, which led to an estimated loss of \$309 million in agricultural production from March 2020 to March 2021 [13], [14]. On the other hand, global urbanization has been transforming rural areas, causing 68% of the population to reside in urban environments by 2050 (United Nations). which would further increase the labor shortage in agriculture. On top of that, labor costs on specialty crop farms in the United States are 3 times higher than the average cost of labor in all U.S. farms (USDA, 2018), which further emphasizes the need for automating labor-intensive operations in apple and other specialty crop fields.

In commercial apple orchards, the demand for labor-intensive fruitlet thinning peaks during the summer months. Figure 1a demonstrates the overcrowding of fruitlet in tree branches as each flower cluster leads to several fruits requiring fruitlet thinning to optimize the number of fruits in each branch based on the branch diameter, sunlight, space, and water. Figure 1b shows farm workers manually thinning apple clusters, a process that is both time-consuming and laborious, requiring a significant number of seasonal workers.

As the U.S. agricultural workforce continues to decline, maintaining competitiveness in the global market necessitates the adoption of labor-saving technologies. Agricultural robots, which can replicate human tasks such as fruitlet thinning during the early growing season, offer a promising solution to labor-intensive operations [17]. In addition to reducing dependence on manual labor, automated and robotic systems for fruit thinning can also contribute to enhancing worker health and safety. Occupational health studies highlight the significant risks associated with manual labor in orchards. For instance, May et al. [18] reveals that farmworkers suffer from a high incidence of musculoskeletal injuries, skin diseases, and other health issues, with the agricultural sector experiencing a fatality rate seven times the national average. Further supporting this need, the study by Earle-Richardson et al. [19] documents the detrimental effects of prolonged physical labor on migrant orchard workers, demonstrating significant decreases in muscle strength within a single workday.

The first crucial step in automating the fruit thinning process is developing a robust vision system capable of detecting green apple fruitlets during the early thinning stage in commercial orchards. Green apple detection is fundamentally an object detection challenge, a domain extensively studied within computer vision. Apple detection systems in orchard environments for possible automation have been reported since the late 90s [20]. In the past, many studies have reported apple detection models for supporting robotic harvesting using traditional image processing techniques such as image color segmentation in RGB, HIS (hue, saturation, and intensity), and/or HSL (hue, saturation, luminance) color spaces [21], [22], [23], [24]. However, the accuracy of these traditional methods has been relatively low, and the approach is limited to a specific environmental condition such as uniform lighting and background conditions created artificially in orchards. It is challenging to implement these image processing algorithms to detect apples in a natural environment with high level of occlusion, fluctuating illumination, and complex backgrounds[25].

During the last few years, machine learning (ML) has become widely adopted for object detection in agriculture, providing more robust detection capabilities with reduced level of image pre-processing and feature extraction [26].

Some of the recent ML models used in detecting apples have been Simple Linear Iterative Clustering (SLIC), Support Vector Machine (SVM) and Random Forest (RF) to detect apples [27], [28].



Figure 1: Fruitlet thinning in commercial orchards: (a) High-density clusters of apple fruitlets on a Scilate apple tree during the peak thinning period in June 2022 (A commercial orchard in Prosser, WA), illustrating the typical overcropping seen in commercial orchards; (b) Top: Laborers utilizing an height-adjustable platform for efficiently thinning fruitlet in various parts of tree canopies; b) Bottom: A worker in a Scifresh apple orchard manually thinning excess fruitlets using an aluminum ladder, a common practice that highlights the labor-intensive nature of this crucial agricultural task.

Additionally, deep learning (DL)-based models have become one of the most effective methods for performing object detection in agriculture as it provides end-to-end processing capability without any manual feature extraction. To perform apple detection in orchards, researchers have implemented DL models such as Faster R-CNN models based on AlexNet and based on ResNet101 [29]. More recently, Kang et al. [30] have purposed a deep-learning-based detector called ‘LedNet’, which is able to perform real-time and accurate apple detection in orchards. The LedNet architecture utilizes the 3-levels feature pyramid network (FPN) and Atrous Spatial Pyramid Pooling (ASPP), a semantic segmentation module used in the feature processing block of the DL module.

Although researchers have been successful in detecting mature apples for robotic harvesting, there are only a few reported studies on the detection of apples during their early growing season for robotic thinning applications. During the early growing season of apples in the natural environment, the color of apples and light reflection is similar to that of leaves, which poses a great challenge in accurately detecting apple fruitlet. Additionally, factors such as occlusion and overlap of fruits with leaves and branches, and uncertain illumination make it difficult to detect fruitlet effectively [31], [32].

Xia et al. [33] used improved Hough transform algorithm and SVM to detect green apples in a natural environment and reported an F1 score of 90.3%. The author used an iterative threshold segmentation (ITS) algorithm to detect regions of interest (ROI) that contained potential apple fruitlet pixels. However, this technique was limited to detecting only non-overlapping apples. Recently, to detect young apples, Tian et. al [34] implemented a YOLOv3 model called ‘Densenet’ and reported an F1 score of 83.2%. Additionally, to detect apples, Huang et al. [35] recently used an improved YOLOv3 model based on the CSPDarknet53 DL network. The study reported an inference speed of 8.6 ms

in detecting immature apples. However, F1 and mAP achieved by the proposed model were only 0.65 and 0.67. Most recently, Wang et al. [36] presented a YOLOv5s-based deep learning technique to detect apple fruitlet before thinning activity in the natural environment. The author of this study implemented transfer learning through a channel pruned YOLOv5s object detection model and fine-tuned the model to achieve a higher detection rate. However, the model size implemented in this study was very small (1.4MB) and the author reported a false detection of 4.2%.

Recent advancements in deep learning models for object detection have significantly enhanced fruitlet detection performance in field environments. The You Only Look Once (YOLO) framework, modified for specific agricultural needs, has shown promising results. For instance, [40] reported that a tailored YOLO model improved the detection of green citrus in complex orchard environments with a substantially better accuracy and speed compared to YOLO v4 [37]. Similarly, a lightweight version of YOLOv8 was developed for detecting pomegranate fruitlets, achieving high precision with reduced model complexity, making it suitable for mobile devices [38]. Additionally, a channel-pruned YOLO V5s model effectively detected apple fruitlets under varying conditions, outperforming several methods while maintaining a compact size for potential use in mobile fruit thinning terminals[39].

Similarly, an adaptation of the YOLOX-m model, optimized for robust feature extraction and enhanced by a feature fusion pyramid network with an Atrous Spatial Pyramid Pooling (ASPP) module, has shown improvements in detecting fruitlets. The ASPP module-based network achieved an average precision of 64.3% for apples and 74.7% for persimmons, outperforming several common detection models and providing a solid reference for diverse fruit and vegetable detection tasks [40]. Similarly, the YOLO-P model, a modified version of YOLOv5 designed specifically for pear detection in orchards, incorporated advanced architectural changes such as shuffle blocks and a convolutional block attention module (CBAN). These modifications improved feature extraction capabilities, allowing the model to perform well under challenging environmental conditions including complex backgrounds and varied lighting. This model not only supports rapid and precise pear detection but also offers insights for enhancing fruit detection systems in similar unstructured environments [41].

Moreover, a YOLO v4-based method specifically tailored for fig detection in dense foliage has shown improvements over previous models including Faster R-CNN, emphasizing YOLO's capability in challenging conditions [42]. YOLOv8 has also been successfully applied to size immature green apples using geometric shape fitting techniques, showcasing high precision and robustness against occlusions in orchard environments [4]. Furthermore, an enhanced YOLOv8 model has proven to be effective for detecting Yunnan Xiaomila peppers, integrating attention mechanisms and deformable convolutions to handle small targets against complex backgrounds [43]. Additionally, modifications to YOLOv5 have improved plum recognition, adapting the algorithm to handle fruit occlusions and environmental variability [44]. Another study with YOLOv7-based model equipped with attention mechanisms and specialized pooling has shown to achieve high precision in detecting plums in natural settings [45].

In orchard automation, YOLO object detection models have been pivotal in enhancing the accuracy and efficiency of fruit detection [4], [46], [47], flower identification [48], [49], [50], and automated harvesting processes [51], [52], [53]. These models adeptly identify and classify fruits at various stages of ripeness, detect flowers with high precision, and facilitate efficient harvesting operations. The development of YOLO models has introduced significant improvements specifically tailored to meet the challenges faced in agricultural environments. For instance, the introduction of multi-scale predictions in YOLOv5 has improved the detection of small and clustered objects like flowers and young fruits, which are crucial during the early stages of crop yield management [54].

The rapid advancement of YOLO-based models has significantly enhanced their precision and processing speeds, vital for implementing robotic solutions such as fruitlet thinning in orchards. Given these swift innovations, continuous evaluation of newer models is essential to harness these improvements for agricultural automation.

This study provides a comprehensive evaluation of the latest YOLO versions: YOLOv10, YOLOv9, and YOLOv8, targeting fruitlet detection in commercial apple orchards by examining 17 configurations across these models and utilizing a commercial orchard's dataset of RGB images from an iPhone 14 across four apple varieties: Scifresh, Scilate, Honeycrisp, and Cosmic Crisp. Each image was annotated with a complete count of visible and occluded apples directly observed in the field, providing a comprehensive dataset for validation. The study also validates the top-performing models using machine vision sensors from Microsoft Azure and Intel Realsense, specifically targeting the Golden Delicious and Scifresh varieties.

2. YOLO Background and Overview: Insights into YOLOv8, YOLOv9, and YOLOv10 Models

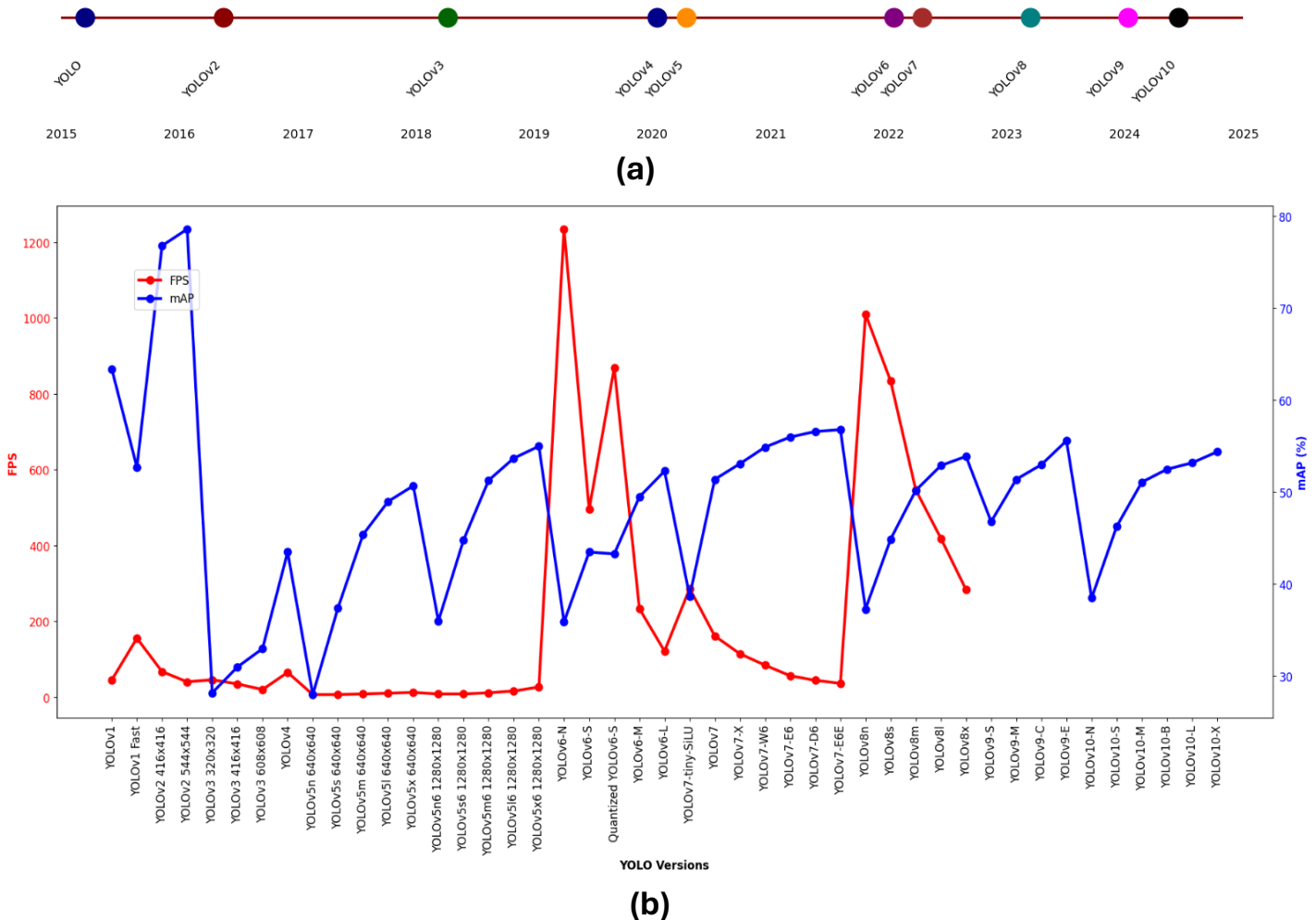


Figure 2: Evolution of YOLO and Performance of YOLO models from 2015-2024: (a) Timeline of YOLO version releases, showcasing advancements from YOLOv1 to YOLOv10. (b) Performance analysis of YOLO models, comparing speed (FPS) and accuracy (mAP) across versions from YOLOv1 to YOLOv10.

Figure 2a shows the timeline history of the YOLO from its release to upto date version as YOLOv10. The YOLO object detection algorithm was first introduced by Joseph Redmon et al. [55] in 2015, revolutionized real-time object detection by combining region proposal and classification into a single neural network, significantly reducing computation time. YOLO's unified architecture divides the image into a grid, predicting bounding boxes and class probabilities directly for each cell, enabling end-to-end learning [55]. YOLO is versatile, and its real-time detection capabilities have revolutionized not only agriculture [56], but also many other field such as medical object detection [57], autonomous vehicle industry[58], security and surveillance systems [59], and industrial manufacturing [60] where accuracy and speed are paramount. The current state-of-the-art iteration of YOLO version is YOLOv10, and Figure 2b shows the FPS and mAP of each model starting from YOLOv1 to YOLOv10.

After the release of first YOLO version, YOLOv2, or YOLO9000 [61], [62], expanded on this foundation by improving the resolution at which the system operated and by being capable of detecting over 9000 object categories, thus enhancing its versatility and accuracy. YOLOv3 further advanced these capabilities by implementing multi-scale predictions and a deeper network architecture, which allowed better detection of smaller objects[63] . The series continued to evolve with YOLOv4 and YOLOv5, each introducing more refined techniques and optimizations to improve detection performance (i.e., accuracy and speed) even further [64], [65]. YOLOv4 incorporated features like Cross-Stage Partial (CSP) connections and Mosaic data augmentation, while YOLOv5, developed by Ultralytics, brought significant improvements in terms of ease of use and performance, establishing itself as a popular choice in the computer vision community. Subsequent versions, YOLOv6 through YOLOv10, have continued to build on this success, focusing on enhancing model scalability, reducing computational demands, and improving real-time performance metrics . Each iteration of the YOLO series has set new benchmarks for object detection capabilities and significantly impacted various application areas, from autonomous driving and traffic monitoring to healthcare and industrial automation..

Starting with YOLOv1, the foundational model introduced significant capabilities with an mAP of 63.4%, although it experienced higher latencies[64] .This was followed by YOLOv2 and YOLOv3, which further improved detection accuracy, achieving mAPs of 76.8% and 57.9%, respectively, at the cost of increased latency. YOLOv4 continued this trend, reaching an mAP of 43.5% and serving as a bridge to more refined models. YOLOv5 emerged as a popular choice, balancing performance and efficiency with a competitive mAP of 50.7% and a latency of 140 ms [66]. The YOLOv6 series, including variants from YOLOv6-N to YOLOv6-L, offered mAP scores ranging from 37.0% to 51.8%, with moderate latencies, marking a significant milestone in optimizing detection speed and accuracy [67]. Lastly, YOLOv7, including the YOLOv7-tiny and standard YOLOv7 models, achieved mAPs of 56.4% and 51.2% respectively, but with significantly higher latencies, indicating a shift towards prioritizing accuracy over speed.

Likewise, YOLOv8 demonstrates commendable performance with mAP scores ranging from 37.3% to 53.9%, and latencies between 6.16 ms to 16.86 ms. While it made significant strides, YOLOv8 falls slightly short in terms of efficiency and accuracy when compared to its successors. Progressing to YOLOv9 [68], this iteration includes models like YOLOv9-N, YOLOv9-S, YOLOv9-M, YOLOv9-C, and YOLOv9-X, which achieve mAP scores from 39.5% to 54.4% [68]. Although YOLOv9 matches YOLOv10 in top mAP scores, its latency figures, particularly for YOLOv9-X, are higher, reflecting lesser efficiency than YOLOv10. This discrepancy highlights YOLOv10's advancements in balancing high accuracy with reduced computational demands. The latest in the lineup, YOLOv10 [69], introduces a range of variants: YOLOv10-N, YOLOv10-S, YOLOv10-M, YOLOv10-B, YOLOv10-L, and YOLOv10-X offering precision scores from 38.5% to 54.4% on the MS-COCO dataset. Notably, YOLOv10-N and YOLOv10-S boast the lowest latencies at 1.84 ms and 2.49 ms, respectively, optimizing them for real-time applications. YOLOv10-X not only achieves the highest mAP of 54.4% but does so with a remarkably low latency of 10.70 ms, demonstrating a significant leap in enhancing both accuracy and inference speed over previous models [69].

YOLOv8 introduced enhancements to its backbone network with an upgraded version of the Darknet architecture, which improved computational efficiency and feature extraction. This version also added layers and refined the loss functions to handle class imbalances and stabilize training outcomes, making it suitable for real-time applications with strict latency demands [67].

YOLOv9 stands out in the realm of real-time object detection with its strategic architectural innovations aimed at overcoming the challenges of information loss in deep neural networks, a critical factor in maintaining detection accuracy and system efficiency. Central to YOLOv9's design is the implementation of the Information Bottleneck Principle and Programmable Gradient Information (PGI), which ensure that crucial data is preserved throughout the layers of the network. This approach facilitates better model convergence by maintaining reliable gradient generation across the network's depth. Further enhancing YOLOv9's capabilities is the integration of Generalized Efficient Layer Aggregation Network (GELAN) and reversible functions. GELAN optimizes the model's computational blocks for flexible performance across various applications, boosting both parameter utilization and efficiency. Meanwhile,

reversible functions address the core issue of information degradation in deep learning architectures; these functions allow the model to invert transformations without any loss, preserving integral data necessary for accurate object detection. This property is especially beneficial in ensuring that YOLOv9 maintains complete information flow, crucial for precise updates to model parameters and effective learning. Figure 3a, b and c show the architecture diagram of YOLOv8, YOLOv9 and YOLOv10 respectively.

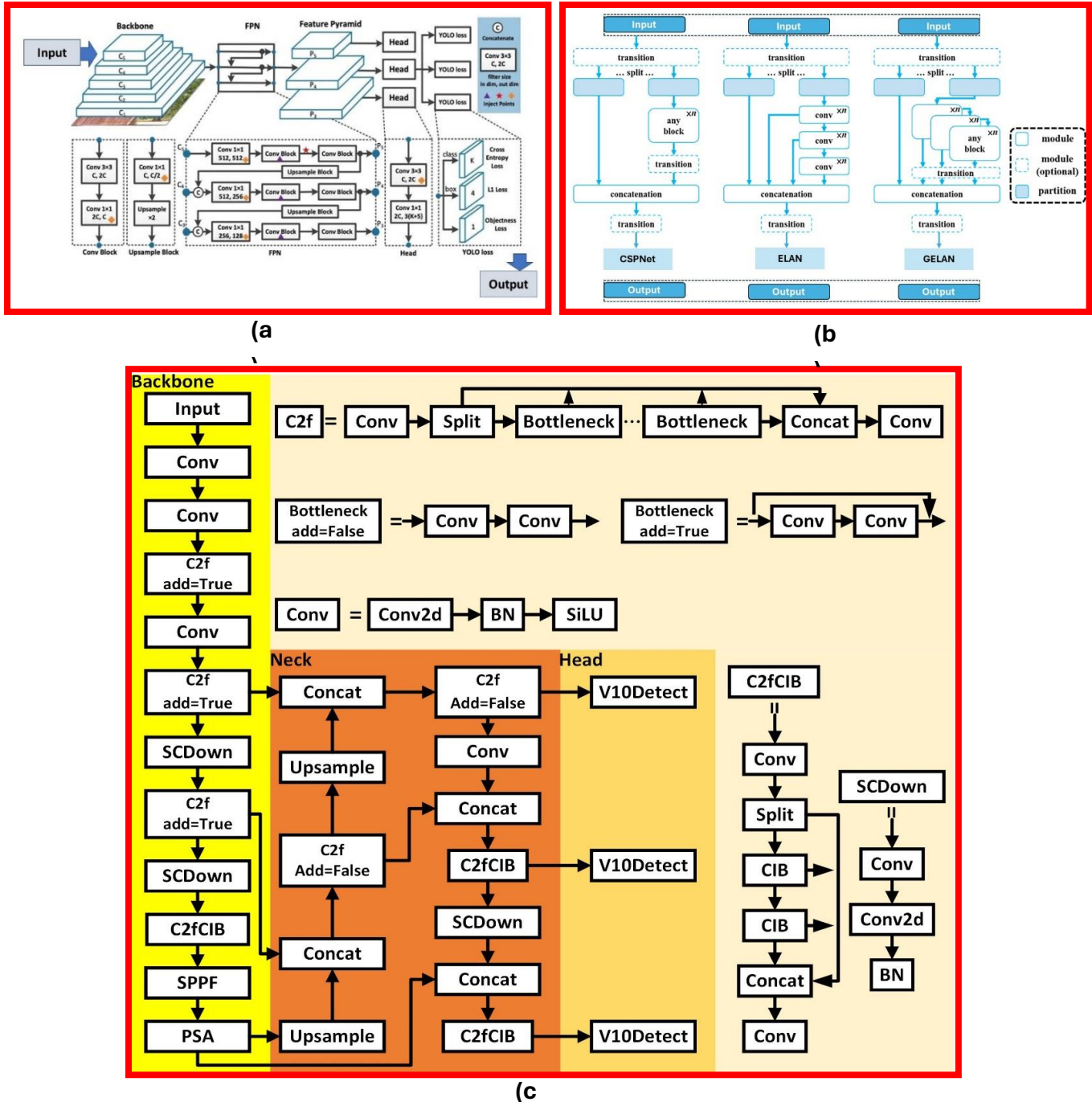


Figure 3: Architecture diagrams of YOLOv8, YOLOv9 and YOLOv10 object detection algorithms: (a) YOLOv8 architecture integrates a convolutional backbone and a Feature Pyramid Network for enhanced multi-scale detection ; (b) YOLOv9 architecture incorporates CSPNet, ELAN, and GELAN modules to optimize feature integration and computational efficiency; and (c) YOLOv10 architecture advances with a dual label assignment strategy and a Path Aggregation Network, improving precision in object localization and classification.

YOLOv10 [69] further optimized the accuracy and speed of object categorization and localization in images. This latest iteration of the YOLO series effectively addresses previous architectural limitations and the reliance on Non-Maximum Suppression (NMS), enhancing both performance and operational efficiency. The architecture of YOLOv10 is distinguished by its enhanced backbone which employs an updated version of CSPNet. This refinement is designed to improve gradient flow and reduce computational redundancy, which is crucial for efficient and precise feature extraction. Additionally, the incorporation of a Path Aggregation Network (PAN) within the neck of the model facilitates effective multi-scale feature fusion.

Another significant innovation in YOLOv10 is its dual-head design. During training, the One-to-Many Head generates multiple predictions per object to provide rich supervisory signals, enhancing learning accuracy. In contrast, during inference, the One-to-One Head delivers a single, optimal prediction per object, eliminating the need for NMS and thereby reducing latency and streamlining the detection process. YOLOv10 also introduces several key features aimed at boosting efficiency and accuracy. The model employs a NMS-free training protocol through consistent dual assignments, dramatically reducing post-processing time and simplifying the output stage. Comprehensive optimizations across the model include lightweight classification heads, spatial-channel decoupled down sampling, and a rank-guided block design. Furthermore, the incorporation of large-kernel convolutions and partial self-attention modules enhance performance without a substantial increase in computational demands.

3. Methods

This study was conducted across commercial orchards in Pullman, Prosser, and Naches, Washington State, USA, over the years 2022 to 2024. It focused on evaluating datasets of green apples, featuring varieties such as Scifresh, Scilate, Cosmic Crisp, Honeycrisp, and Golden Delicious. RGB images for this study were captured using IntelRealsense machine vision camera and were manually labeled to prepare the constant dataset for training of each configuration across YOLOv8, YOLOv9, and YOLOv10 models. In total, 17 model configurations were examined: 5 for YOLOv8,

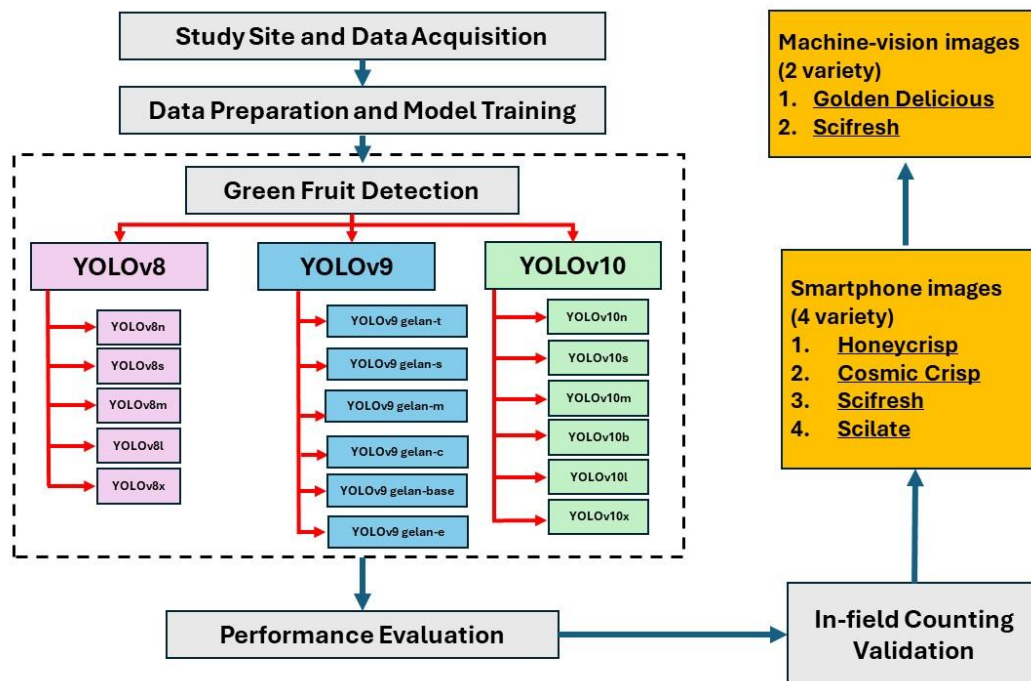


Figure 4: Flow diagram of this study of comparison of YOLOv8, YOLOv9 and YOLOv10 illustrating the study's methodology, including data collection, model training, and validation across multiple sensors and apple varieties in commercial orchards

6 for YOLOv9, and 6 for YOLOv10. All model configurations were trained under standardized hyperparameter settings on the same computational system to ensure consistency and comparability. Validation of these models involved additional RGB images captured from various orchards using an Apple iPhone 14 smartphone.

This validation process aimed to assess each model's fruit counting accuracy against manually counted ground truths, which included scenarios with occluded apples. Furthermore, this validation step was designed to rigorously test the highest-performing models in terms of speed and accuracy using images from different sensors. The details of this comprehensive methodology are illustrated in Figure 4, providing a visual reference for the experimental setup and data collection approach employed in this study.

3.1 Study Site and Data Acquisition

The primary data collection for this study was conducted at Allan Brothers Orchard in Prosser, Washington State, USA, focusing on datasets of immature green apples for training models. RGB images were acquired using an Intel RealSense 435i camera during June 2024. For validation, additional datasets were collected from different locations and times: Cosmic Crisp apple images from the ROZA experiment station at WSU IAREC in Prosser, Honeycrisp apple images from an orchard in Naches owned by Allan Brothers Fruit Company, and Golden Delicious apple images from Pullman, collected on June 14, 2022. Furthermore, validation of apple counts using the Intel RealSense camera and Microsoft Azure camera was conducted in June 2023 and June 2022 respectively. All images were captured prior to the manual thinning process conducted by orchard workers. The details of each machine vision sensor used in data collection of this study are:

Intel RealSense D435i: This camera features a 2-megapixel RGB sensor capable of capturing high-quality images. Operating at a resolution of 1280×720 pixels, it provides a comprehensive view with a 69.4° horizontal and 42.5° vertical field-of-view, ensuring broad coverage in various environments. The Intel RealSense D435i is designed to be compact and lightweight, making it highly effective for capturing RGB data in diverse settings.

Microsoft Azure Kinect DK: Equipped with a 12-megapixel color camera, this sensor delivers exceptional image clarity and detail. The RGB camera component of the Azure Kinect DK sensor excels in a range of lighting conditions, enhancing its utility in natural orchard environments where lighting can vary. The device's high-resolution imaging capabilities make it ideal for detailed visual data collection in agricultural research.

Apple iPhone14: The Apple iPhone 14 features an advanced 12-megapixel RGB camera that excels in capturing high-resolution images with remarkable clarity and color accuracy. Its sophisticated sensor and computational photography capabilities enable detailed and vibrant image capture, making it ideally suited for collecting visual data in various lighting conditions, crucial for applications such as agricultural monitoring and research.

3.2 Data Preparation and Model Training

A total of 1,147 images were manually annotated with bounding boxes using the online labeling platform provided by Roboflow. These images were allocated into training and validation at the ratio of 8:2 respectively, facilitated by Roboflow's distribution tools. No image preprocessing steps were undertaken in this study, as the objective was not to enhance any specific model but rather to compare and evaluate the performance of these models using raw data collected in natural orchard settings.

The computational analyses for this study were conducted on a high-performance workstation equipped with an Intel Xeon(R) W-2155 CPU, featuring a base clock speed of 3.30 GHz across 20 cores. This setup provided substantial processing power necessary for handling intensive data processing tasks. The workstation was also outfitted with NVIDIA Corporation GP102 [TITAN Xp] graphics cards, enhancing its ability to perform complex image processing and machine learning tasks efficiently. The system included a substantial storage capacity of 7.0 TB, facilitating

extensive data management and analysis. It operated under Ubuntu 20.04.6 LTS, a robust and stable 64-bit operating system, using GNOME version 3.36.8 for its graphical interface and X11 as its windowing system.

The analysis of YOLOv8, YOLOv9, and YOLOv10 encompassed a total of 17 configurations (five for YOLOv8, six for YOLOv9, and six for YOLOv10). Each model configuration was rigorously tested for precision, recall, mAP@0.5, and image processing speed. For the training of all models, a consistent configuration was rigorously maintained to ensure uniformity and comparability across experiments. Each model was trained for 700 epochs, reflecting a substantial duration to adequately learn and adapt to the dataset's complexities. The batch size was set at 8, optimizing the balance between memory usage and processing speed. Images were resized to a uniform resolution of 640x640 pixels to standardize the input data size across all models. The Stochastic Gradient Descent (SGD) optimizer was employed to update model weights effectively, favored for its efficiency in handling large-scale and complex data. Additionally, the configuration threshold for confidence was set at 0.25, and the Intersection over Union (IoU) threshold was maintained at 0.7, criteria chosen to optimize the balance between precision and recall during object detection tasks.

The hyperparameter settings outlined in table 1 provide a detailed framework for optimizing the training of YOLO models in the study. Key parameters such as the initial and final learning rates were set at 0.01, facilitating a controlled adjustment of learning throughout the training process. Momentum was maintained at 0.937 to ensure consistent updates across epochs, while a minimal weight decay of 0.0005 helped prevent overfitting. The training initiated with a warmup phase spanning 3 epochs to stabilize the learning parameters early in the training. Loss adjustments were specifically tuned, with box loss, class loss, and definition loss set at 7.5, 0.5, and 1.5 respectively, to balance the contributions of different components of the loss function. Image augmentation techniques such as hue, saturation, and value adjustments were precisely defined to enhance model robustness under varied lighting conditions typically found in orchard environments. Specific settings for geometric transformations like rotation, translation, and scaling were employed to simulate different orientations and sizes of objects, crucial for improving the model's ability to generalize across diverse scenarios. The table also highlights the use of flipping and mosaic data augmentation to further enrich the training dataset, ensuring comprehensive exposure to potential real-world variations.

Table 1: Hyperparameter Settings for YOLOv8, YOLOv9, and YOLOv10 used in training YOLO models for fruitlet detection in commercial apple orchards

Hyperparameter	Value	Description
Initial Learning Rate (<i>lr0</i>)	0.01	Sets the starting learning rate.
Final Learning Rate (<i>lrf</i>)	0.01	Determines the learning rate at the end of training.
Momentum	0.937	Controls the momentum for the SGD optimizer
Weight Decay	0.0005	Helps in regularizing and preventing overfitting.
Warmup Epochs	3.0	Number of initial epochs for learning rate stabilization.
Box Loss Gain (<i>box</i>)	7.5	Weight of the bounding box loss component.
Class Loss Gain (<i>cls</i>)	0.5	Weight of the class prediction loss component.
Definition Loss Gain (<i>dfl</i>)	1.5	Weight of the definition loss component

3.3 Performance Evaluation

To evaluate the detection capabilities of each configuration of YOLOv8, YOLOv9, and YOLOv10, the metrics of precision, recall, and mean Average Precision at Intersection over Union (IoU) threshold of 0.50 (mAP@50) were employed. Precision was calculated as the ratio of true positive detections to the total predicted positives, given by equation 1, where TP denotes true positives and FP denotes false positives. Recall measured the ratio of true positive detections to the actual positives, formulated as equation 2 where FN represents false negatives. The mAP@50 was determined by averaging the precision across all recall levels for an IoU > 0.50. Additionally, the image processing speed for each model was analyzed and compared across three categories: preprocessing, inference, and postprocessing. These evaluations were systematically conducted across 17 configurations of the YOLO models: YOLOv8m, YOLOv8s, YOLOv8l, YOLOv8x, YOLOv8c for YOLOv8; YOLOv9 Gelan-e, YOLOv9 Gelan-c, YOLOv9 Gelan-s, YOLOv9 Gelan-t, YOLOv9 Gelan-m, and YOLOv9 Gelan for YOLOv9, and YOLOv10m, YOLOv10s, YOLOv10l, YOLOv10x, YOLOv10c, YOLOv10d for YOLOv10, to evaluate their efficiency in detecting fruitlets in commercial orchards.

$$Precision = \frac{TP}{TP + FP}$$

Equation 1

$$Recall = \frac{TP}{TP + FN}$$

Equation 2

Additionally, the assessment involved analyzing preprocessing, inference, and postprocessing speeds for each model configuration, as these metrics are critical for real-time object detection systems. Preprocessing speed determines how quickly a model can prepare images for detection, inference speed measures the time taken to identify objects within images, and postprocessing speed reflects how swiftly the model finalizes the outputs after detection. Each of these stages is essential for efficient operation in agricultural applications, where timely and accurate detection can significantly impact decision-making and resource management. The computational efficiency of these models directly influences their practical utility in automated fruit detection systems, making this evaluation crucial for advancing agricultural technology solutions.

3.4 In-Field Counting Validation

Upon evaluating the performance metrics of each YOLOv8, YOLOv9, and YOLOv10 configuration for detecting fruitlets, the most effective model from each version was selected based on the highest accuracy achieved at mAP@0.5. These top-performing models from YOLOv8, YOLOv9, and YOLOv10 were further validated to assess their detection capabilities in a real commercial orchard setting across five distinct apple varieties in Washington State. This validation process utilized images collected both by smartphone and machine vision sensors. Initially, images of Scifresh, Scilate, Cosmic Crisp, and Honeycrisp apples were captured using an iPhone 14. A total of 128 images, 32 per variety, were analyzed to evaluate the models' counting accuracy before the thinning process.

Subsequently, an additional set of images was used for further validation. This included 32 images of Golden Delicious apples captured using a Microsoft Azure camera, and another 32 images of Scifresh apples taken with an IntelRealsense camera. Notably, while the IntelRealsense camera images of Scifresh and Scilate apples served as the training dataset, validation focused on varieties like Golden Delicious, Cosmic Crisp, and Honeycrisp, which were not included in the training phase. For each image, a meticulous count of all visible and occluded apples was manually performed directly in the field. This comprehensive manual counting provided a precise ground truth for each image sample across the different apple varieties, ensuring robust validation of the models' performance.

In our study assessing the performance of YOLO models for detecting fruitlets in commercial orchards, Root Mean Square Error (RMSE) and Mean Absolute Error (MAE) were employed as crucial metrics to quantify the accuracy of fruit counts predicted by the models compared to manually counted ground truths. RMSE was calculated using the equation 3:

$$RMSE = \sqrt{\left(\frac{1}{n} \sum_{i=1}^n (\text{predicted}_i - \text{actual}_i)^2\right)}$$

Equation 3

Here, predicted_i denotes the number of fruits counted by the model, actual_i represents the manually counted fruits for each image, and n is the total number of images. This measure calculated the square root of the average of the squared differences between predicted and actual counts, emphasizing larger errors by squaring the discrepancies, which made it particularly relevant for highlighting significant deviations in model performance.

Likewise, MAE was determined using equation 4:

$$MAE = \left(\frac{1}{n}\right) * \sum_{i=1}^n |\text{predicted}_i - \text{actual}_i|$$

Equation 4

Where, predicted_i and actual_i denotes the retain their definitions, with MAE calculating the average of the absolute differences between the predicted and actual counts. This metric, being less sensitive to large errors compared to RMSE, provided a straightforward indication of the average error magnitude per image, offering an intuitive measure of prediction accuracy across the dataset.

4. Results and Discussion

The evaluation of performance across different YOLO model configurations: YOLOv8, YOLOv9, and YOLOv10 is comprehensively illustrated in Figures 5, 6, and 7, respectively. Figure 5a presents an original image showcasing green apples in a complex orchard environment characterized by shadow and partial sunlight, set against an all-green background. This setting represents a challenging scenario for object detection due to the camouflaging color palette and varying light conditions. Figure 5b details the performance of the YOLOv8l model configuration, where a false detection has occurred. Notably, a double bounding box is erroneously placed over a region obscured by trellis wire and leaves, mistakenly identified as fruitlets. This misidentification is highlighted by a yellow circle, indicating the area of false positive detection. Figure 5c illustrates the results from the YOLOv8m configuration, which also resulted in a double detection over a single green apple. This overprediction is marked by a yellow dotted circle, showcasing the model's sensitivity to overlapping features within the detection area.

Figure 5d captures the detection outcomes from the YOLOv8x model, which successfully identified five apples accurately in the described complex conditions. This model's effectiveness in handling the intricacies of the environment underscores its robustness. Figures 5e and 5f depict the performances of the YOLOv8n and YOLOv8s configurations, respectively. Both configurations have correctly identified the green apples, demonstrating their capability to accurately detect objects without the interference observed in other configurations.

Likewise, Figure 6 illustrates the detection performance of various YOLOv9 configurations across a challenging orchard environment, comparing them against earlier YOLOv8 results. The configurations YOLOv9 Gelan-c (subfigure a), YOLOv9 Gelan-e (subfigure b), YOLOv9 Gelan-s (subfigure c), YOLOv9 Gelan-t (subfigure d), and YOLOv9 Gelan base (subfigure f) all demonstrated excellent accuracy in identifying fruitlets, with no false detections noted. However, an exception was observed in YOLOv9 Gelan-m (subfigure e), which uniquely recorded a false positive.

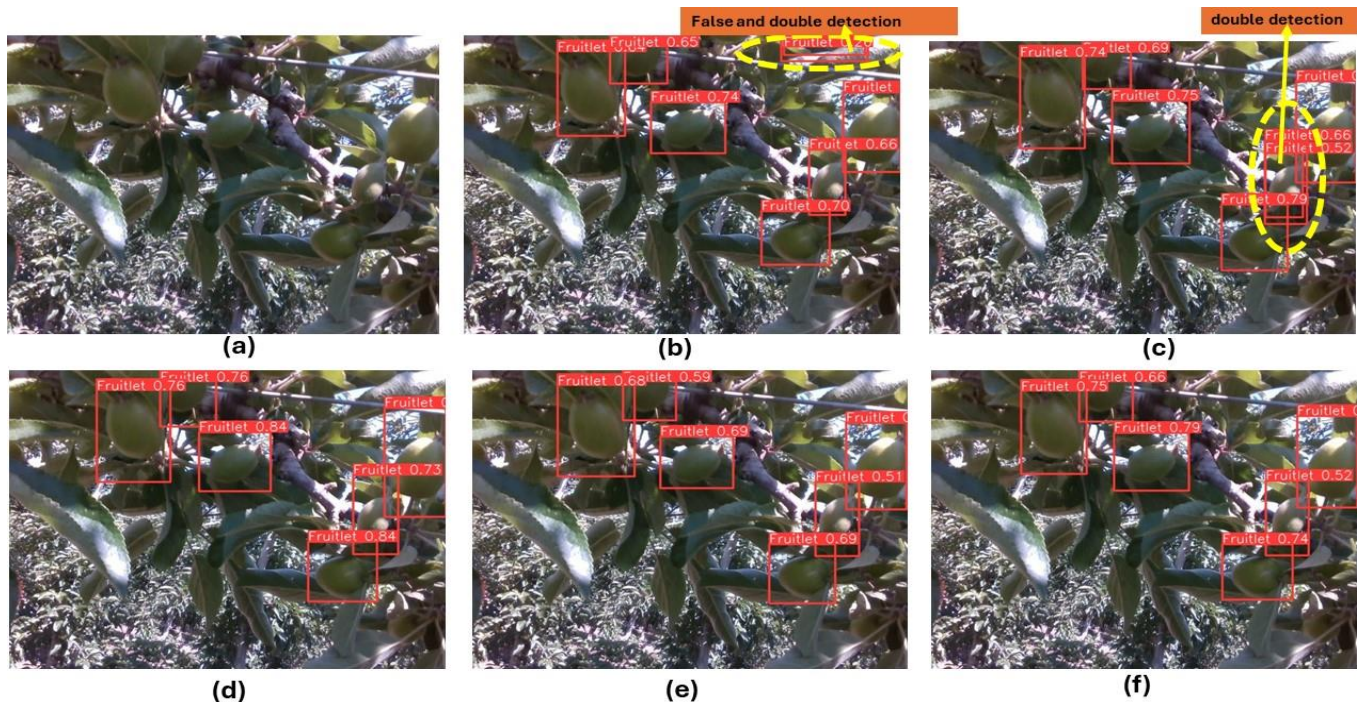


Figure 5: Illustration of comparative performance of YOLOv8 object detection algorithm for fruitlet detection in a complex orchard environment: a) Original Image; b) YOLOv8l detection results; c) YOLOv8m detection results ; d) YOLOv8n detection results ; e) YOLOv8s detection results ; and e) YOLOv8x detection results

Figure 7 showcases the detection capabilities of the YOLOv10 object detection algorithm on the same original image previously analyzed in Figures 5 and 6. Subfigure 7a highlights a scenario where YOLOv10b mirrors the false detection previously observed with YOLOv8l (Figure 5b), incorrectly identifying a non-fruit area as containing fruitlet with a single bounding box. This misidentification underscores potential challenges in distinguishing complex background elements from target objects under certain conditions. In contrast, the configurations YOLOv10l, YOLOv10n, and YOLOv10s achieved accurate detection results, comparable to the performance of YOLOv8n, YOLOv8s, YOLOv8x, YOLOv9 Gelan-c, and YOLOv9 Gelan-e as depicted in Figures 5e, 5f, and 6. These results indicate a refined ability to accurately identify fruitlets within complex orchard environments, highlighting improvements in the model's precision and real-time detection capabilities. However, similar to YOLOv10b, YOLOv10m and YOLOv10x (Figures 7c and 7f) repeated the error of detecting non-existent green apples, a persistent issue also noted in YOLOv8 configurations. These instances of over-detection suggest areas for further optimization within the YOLOv10 series, particularly in enhancing the algorithm's discrimination capacity in complex visual scenarios where background and target features closely intersect.

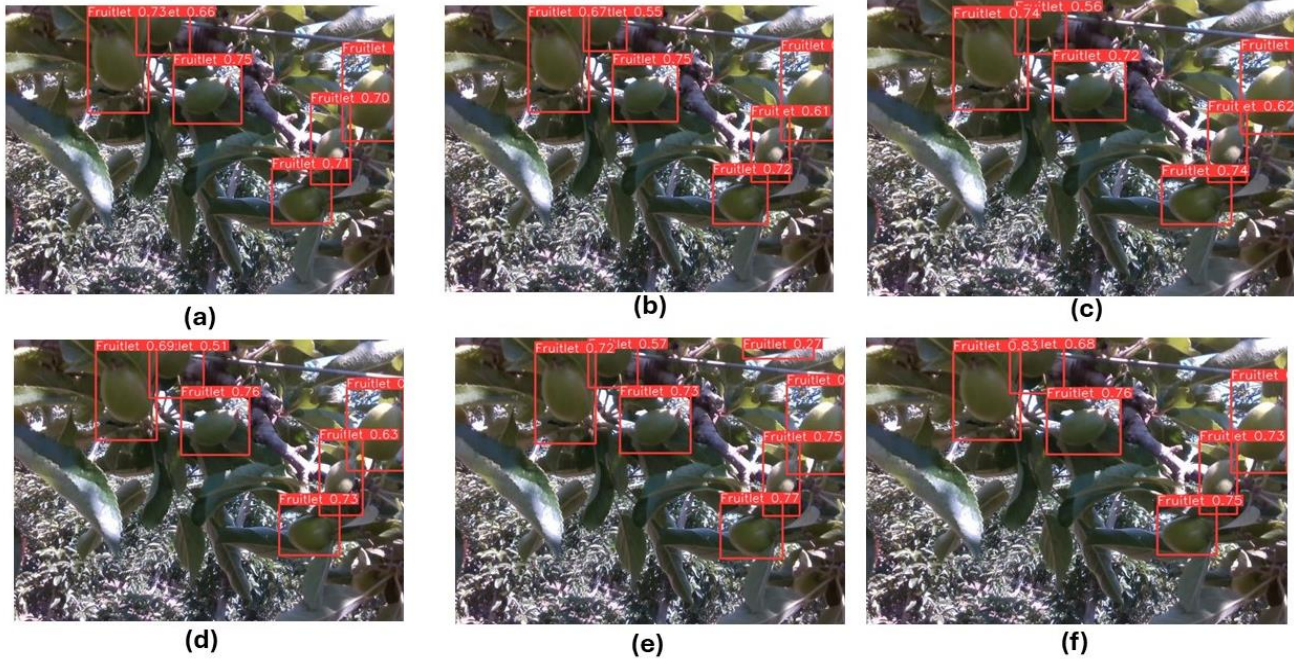


Figure 6: Illustration of comparative Performance of YOLOv9 object detection algorithm for fruitlet detection in a complex orchard environment: a) YOLOv9 gelan-c detection results; b) YOLOv9 gelan-e detection results; c) YOLOv9 gelan-s detection results; d) YOLOv9 gelan-t detection results; e) YOLOv9 gelan-m detection results; and f) YOLOv9 gelan base detection results.

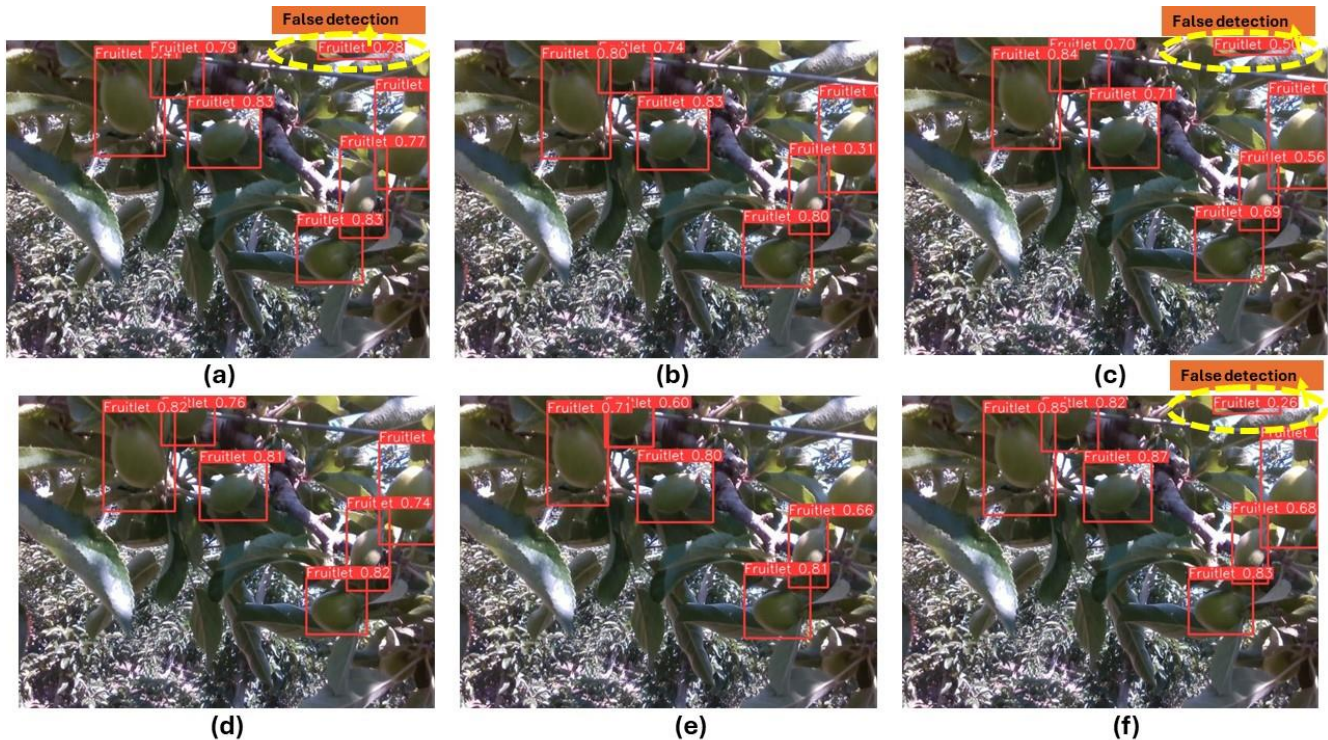


Figure 7: Performance of YOLOv10 object detection algorithm's all configurations for fruitlet detection in a complex orchard environment: (a) YOLOv10b incorrectly detects a non-fruit area as containing fruitlet ; (b) YOLOv10l accurately identifies fruitlets within the orchard. (c) YOLOv10m falsely detects non-existent green apples. (d) YOLOv10-N demonstrates precise fruitlet detection. (e) YOLOv10s successfully identifies fruitlets with high accuracy. (f) YOLOv10x also incorrectly identifies non-existent fruitlets, mirroring the error of YOLOv10b

4.1 Assessment of Detection Accuracy: Precision and Recall Metrics

The comparative analysis of detection accuracy across different YOLO configurations, as illustrated in Figure 8, underscores the nuanced performance variations in precision and recall metrics. Notably, YOLOv9 configurations outperformed others, with YOLOv9 Gelan-c achieving the highest precision (0.903), indicating exceptional accuracy in fruitlet detection while effectively minimizing the misidentification of non-fruits. Conversely, YOLOv9 Gelan-e exhibited the highest recall (0.891), highlighting its ability to capture a larger proportion of true positive samples, though it incurred a slight increase in false positives.

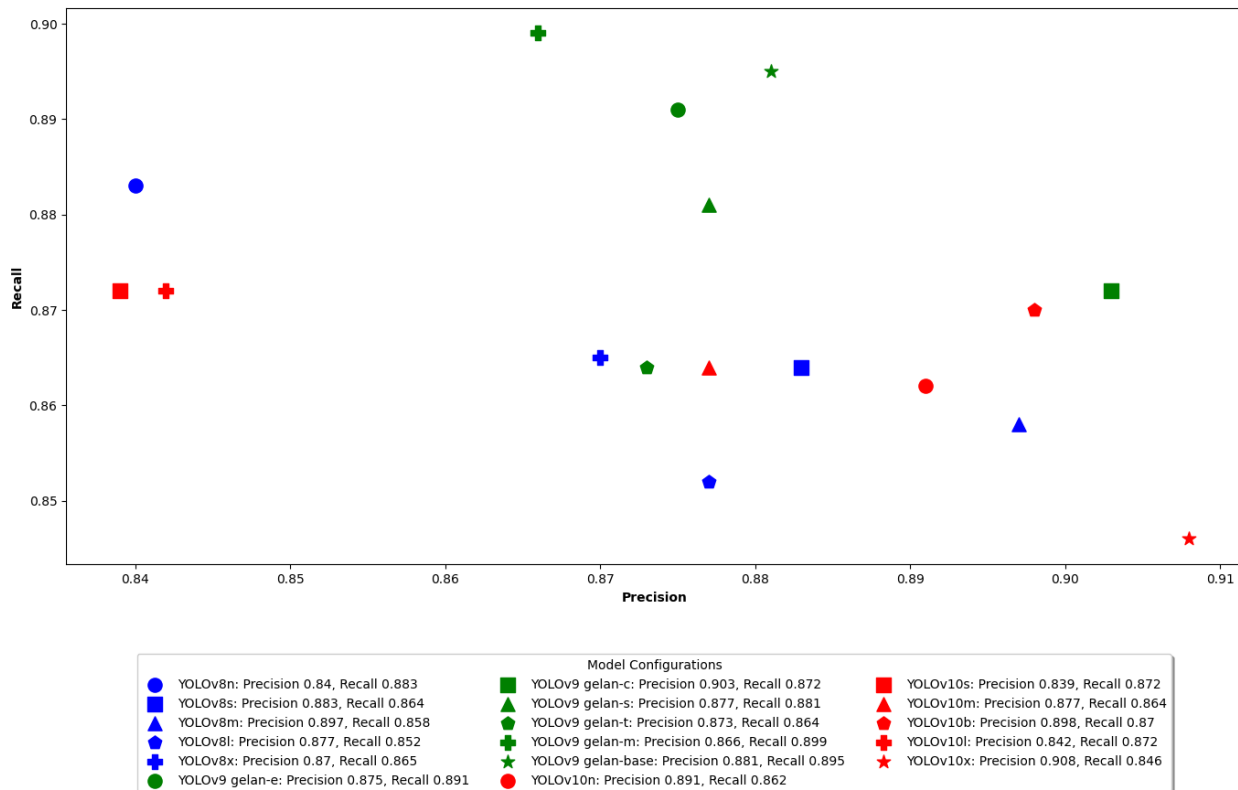


Figure 8: Scatter plot illustrating precision and recall for all configurations of YOLOv8, YOLOv9, and YOLOv10 object detection algorithms for fruitlet detection in complex and commercial apple orchards.

Within the YOLOv8 series, YOLOv8m stood out with the highest precision (0.897), suggesting its superior efficacy in accurately identifying target objects without overflagging. YOLOv8n displayed the highest recall (0.883), which implies it was the most effective at identifying all relevant instances, despite a potential rise in false positives. The other configurations, YOLOv8s, YOLOv8l, and YOLOv8x, demonstrated a balanced trade-off between precision and recall, with precision scores between 0.84 and 0.877 and recall scores ranging from 0.852 to 0.865. For YOLOv10, the configuration YOLOv10x led with the highest precision (0.908), showcasing its accuracy in correctly identifying objects without excessive false detections. However, it showed a relatively lower recall (0.846), indicating some true positives might have been overlooked. YOLOv10b managed a better balance, achieving a recall of 0.87 and precision nearly 0.898, respectively.

Figure 9 showcases the performance metrics of the best-performing YOLO configurations for detecting fruitlets, segmented into subfigures for clarity. Subfigures 9a, 9b, and 9c illustrate the precision, recall, and F1-score, respectively, for YOLOv8n, which outperformed all other YOLOv8 configurations. Subfigures 9d, 9e, and 9f detail the superior performance of YOLOv9 Gelan-e, the best among the six configurations of YOLOv9 tested. Furthermore,

Subfigures 9g, 9h, and 9i present the performance metrics for YOLOv10n, which emerged as the leading configuration in the YOLOv10 series.

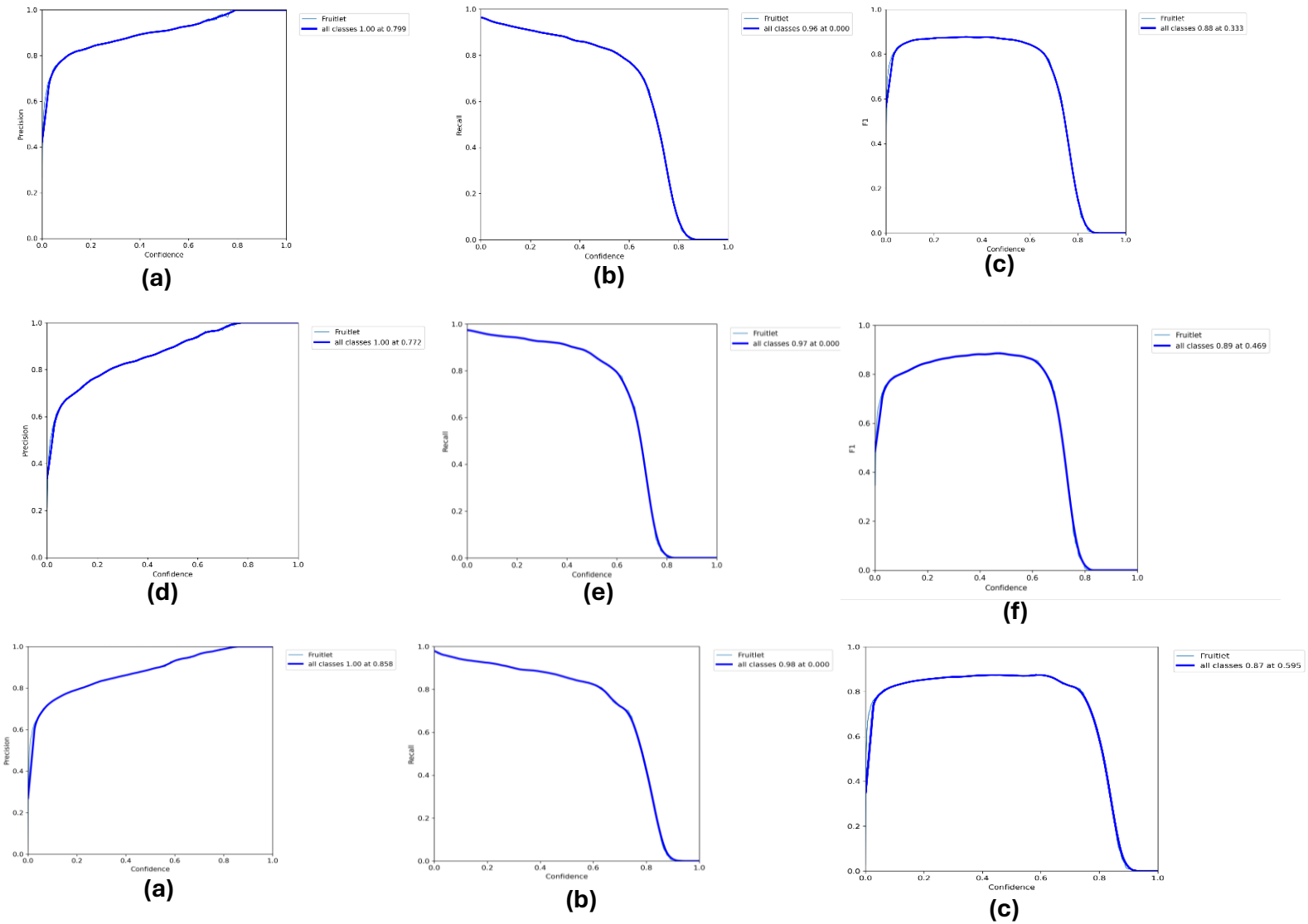


Figure 9: Performance Metrics for the best YOLO Models out of each configuration across YOLOv8, YOLOv9, and YOLOv10 on Fruitlet Detection in complex orchard environments a) YOLOv8n precision confidence curve; b) YOLOv8n recall confidence curve; c) YOLOv8n F1-score curve; d) YOLOv9 gelan-e precision confidence curve; e) YOLOv9 gelan-e recall confidence curve; f) YOLOv9 gelan-e F1-score curve; g) YOLOv10n precision confidence curve; h) YOLOv10n recall confidence curve; i) YOLOv10n F1-score curve.

4.2 Evaluation of Detection Consistency: Mean Average Precision at IoU=0.50

The assessment of mean Average Precision at an Intersection over Union (IoU) threshold of 0.50 ($mAP@0.50$) across various YOLO model configurations in Figure 10 provides profound insights into their efficacy in detecting fruitlets within agricultural settings. Among all evaluated configurations, YOLOv9 models, particularly YOLOv9 Gelan-e and YOLOv9 Gelan-base, stand out with the highest $mAP@0.50$ scores of 0.935 both, respectively. However, all configurations of YOLOv9 achieved higher $mAP@50$ as depicted in Figure 10. These scores not only exceed those achieved by all configurations of YOLOv8 and YOLOv10 but also underscore YOLOv9's superior precision in object detection tasks.

Within the YOLOv10 series, YOLOv10n leads with an $mAP@0.50$ of 0.921, closely followed by YOLOv10b and YOLOv10-M, which record scores of 0.919 and 0.917 respectively. Despite their strong performance, these figures remain slightly below the peak values presented by YOLOv9, indicating that specific enhancements in YOLOv9 have likely boosted its accuracy capabilities. In contrast, the YOLOv8 configurations show a wider spectrum of performance, with YOLOv8s achieving the highest $mAP@0.50$ within its group at 0.924, nearly matching the top-performing configurations of YOLOv10. Nonetheless, configurations such as YOLOv8l and YOLOv8x, with lower scores of 0.912 and 0.914 respectively. This variation may be attributed to an over-parameterization of the models for the given task. Given the simplicity and the fewer categories of the dataset compared to the more complex COCO dataset, the extensive number of parameters in these models may not be necessary and could detract from optimal performance.

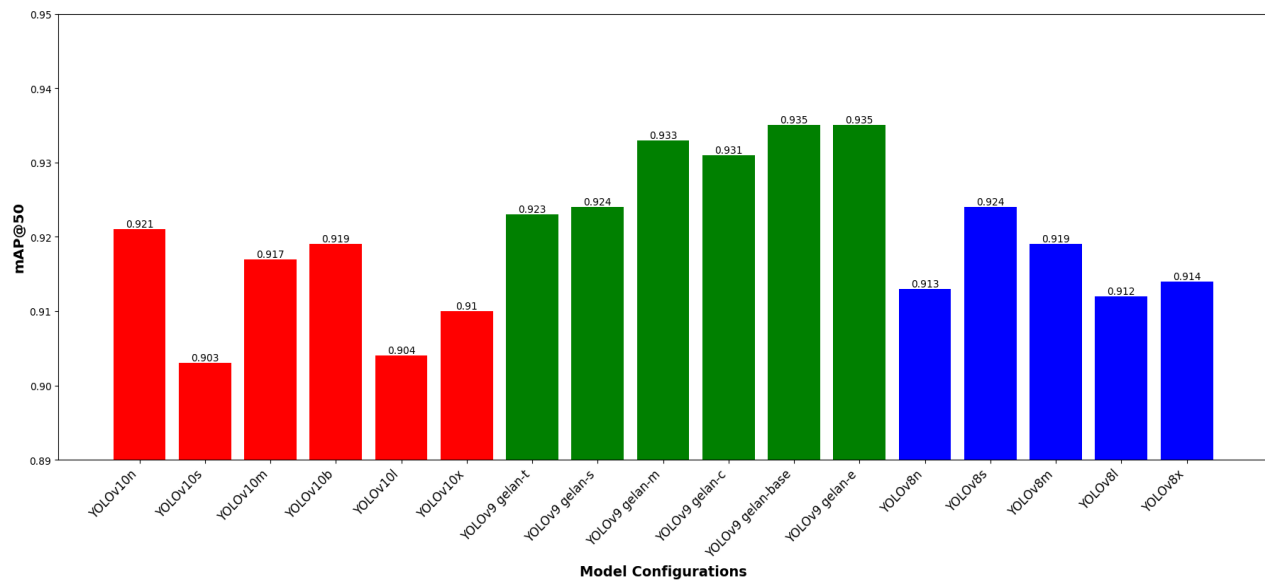


Figure 10: Bar diagram showing $mAP@50$ scores for all 17 Configurations of YOLOv8, YOLOv9, and YOLOv10 for fruitlet detection in commercial orchards.

4.3 Analysis of Computational Efficiency: Image Processing Speed

In the evaluation of computational efficiency, particularly concerning image processing speed, YOLOv8x was observed as the standout configuration, achieving the fastest preprocessing speed at merely 0.9 ms. Theoretically, preprocessing speeds across models should be consistent, and the postprocessing speeds between YOLOv8 and

YOLOv9 are expected to be comparable. The observed discrepancies in preprocessing speed are likely attributable to random errors rather than intrinsic differences between model architectures.

Building on the earlier discussion of preprocessing speeds, YOLOv8 configurations similarly excelled in the inference speed analysis. Notably, YOLOv8n achieved an exceptional inference speed of 4.1 ms, outperforming the fastest configurations from both the YOLOv9 and YOLOv10 series. Specifically, the quickest YOLOv9 configuration, YOLOv9 Gelan-s, recorded an inference speed of 11.5 ms, and the speediest YOLOv10 model, YOLOv10-s, reached an inference time of 5.5 ms. These results (4.1 ms for YOLOv8n, 11.5 ms for YOLOv9 Gelan-s, and 5.5 ms for YOLOv10s highlight a significant performance advantage for YOLOv8n in terms of inference capabilities. This superior performance in computational speed during the critical inference phase emphasizes the robustness of YOLOv8n, suggesting that earlier iterations of the YOLO series, particularly YOLOv8, may still hold a distinct advantage in scenarios demanding high-speed, accurate object detection. Such insights are crucial for optimizing real-time applications where quick decision-making is essential, reaffirming the relevance of YOLOv8 in current technological landscapes. Detailed performance metrics for each configuration across all three YOLO series are systematically presented in Table 2, providing a comprehensive view of their respective computational efficiencies of all configurations of YOLOv8, YOLOv9 and YOLOv10.

Table 2: Computational Speeds of YOLOv8, YOLOv9, and YOLOv10 Configurations for fruitlet detection in complex orchard environments.

YOLO models	YOLO Configuration	Preprocessing Speed (ms)	Inference Speed (ms)	Postprocessing Speed (ms)
YOLOv8	YOLOv8n	1.3	4.1	2.3
	YOLOv8s	1.3	6.4	2.3
	YOLOv8m	1.3	11.2	2.1
	YOLOv8l	1.2	18.7	2.2
	YOLOv8x	0.9	24.8	2.3
YOLOv9	YOLOv9 Gelan-t	1.3	14.1	2.2
	YOLOv9 Gelan-s	1.3	11.5	2.2
	YOLOv9 Gelan-m	1.3	14	2.1
	YOLOv9 Gelan-c	1.3	17	2
	YOLOv9 Gelan-base	1.2	17.2	2
	YOLOv9 Gelan-e	1.1	33.5	1.9
YOLOv10	YOLOv10n	1.4	5.5	1.6
	YOLOv10s	1.3	7.7	1.6
	YOLOv10m	1.3	13	1.6
	YOLOv10b	1.3	16.7	1.5
	YOLOv10l	1.4	19.6	1.5
	YOLOv10x	1.2	26.5	1.5

Note* **P**reprocessing refers to the initial stage where images are prepared for analysis, involving adjustments such as scaling, normalization, and augmentation to optimize them for detection. Inference refers to the core phase of the process where the model analyzes the preprocessed images to detect and identify objects based on the learned features and patterns. Postprocessing refers to the final stage that refines the outputs from the inference, applying techniques like Non-Maximum Suppression (NMS) to eliminate redundant detections and finalize the list of detected objects.

YOLOv10 demonstrated superior performance in postprocessing speeds, setting a new benchmark for rapid image processing completion. Specifically, the YOLOv10n configuration excelled with a postprocessing time of only 1.6 ms, significantly outpacing the fastest configurations from YOLOv9 and YOLOv8. The most efficient YOLOv9 configuration, YOLOv9 Gelan-e, achieved a postprocessing speed of 1.9 ms, while YOLOv8m, the quickest among the YOLOv8 series, recorded a postprocessing time of 2.1 ms. These results (1.6 ms for YOLOv10n 1.9 ms for YOLOv9 Gelan-e, and 2.1 ms for YOLOv8m) distinctly illustrate YOLOv10's edge in finalizing the detection process, showcasing its advanced capabilities in handling the concluding phases of object detection efficiently. Overall, while YOLOv8 configurations outshone both YOLOv9 and YOLOv10 in preprocessing and inference speeds, demonstrating robustness and speed during the initial and middle phases of the detection process, YOLOv10 emerged as the leader

in postprocessing efficiency. This marked advantage in the final phase of image processing by YOLOv10 highlights its optimization for quick output readiness, a crucial factor in real-time applications.

4.4 Field Validation of Counting Accuracy: RMSE and MAE Metrics

For the counting validation performed on four apple varieties images collected using Apple Iphone 14 smartphone, the top-performing configurations from each YOLO version: YOLOv8n, YOLOv9 Gelan-e, and YOLOv10n were

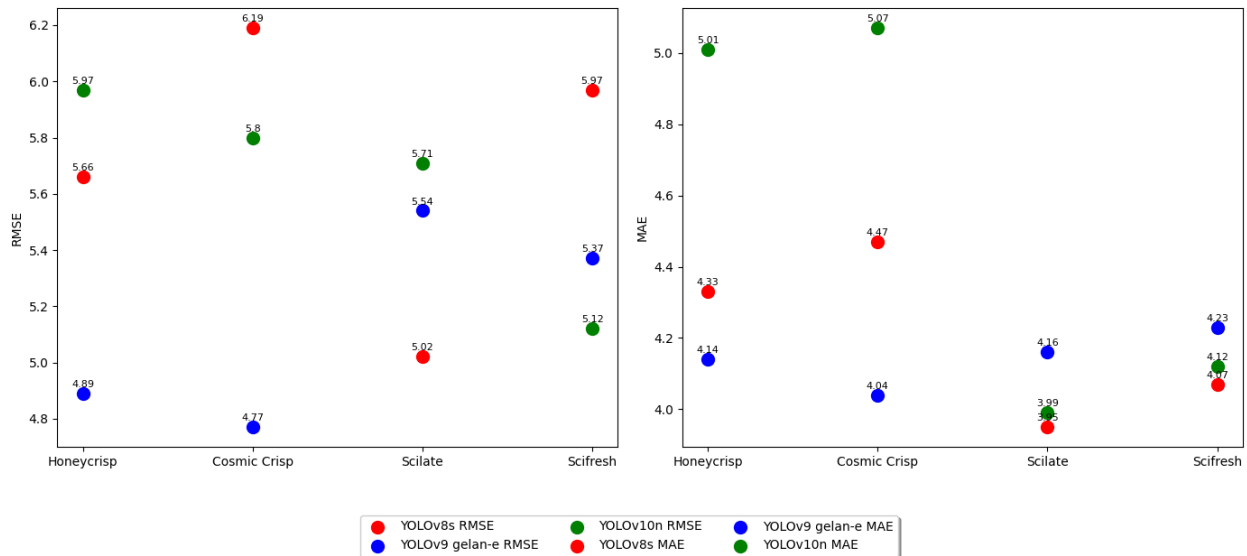


Figure 11: RMSE and MAE for in-field counting validation for Green Apple Detection Using iPhone Images: Comparison of RMSE (left) and MAE (right) for green apple detection across YOLOv8s, YOLOv9 gelan-e, and YOLOv10n configurations, highlighting model accuracy and precision.

rigorously assessed for accuracy in fruit counting.

For Honeycrisp apple variety, the YOLOv9 Gelan-e configuration demonstrated superior performance across several apple varieties, showcasing its effectiveness in precision fruit counting. Specifically, for Honeycrisp apples, it achieved an RMSE of 4.89 and an MAE of 4.14, indicating a high level of accuracy. For Cosmic Crisp, it recorded the lowest RMSE at 4.77 and MAE at 4.04. This trend of superior accuracy continued with Scilate apples, achieving an RMSE of 5.54 and an MAE of 4.16, and for Scifresh apples, it noted an RMSE of 5.37 and an MAE of 4.23. These results affirm YOLOv9 Gelan-e's robust performance, consistently outperforming YOLOv8 and YOLOv10 configurations across diverse apple varieties. Figure 10 shows the detailed distribution visualization of RMSE and MAE for the in-field counting validation of four apple varieties collected using Apple Iphone 14 camera during the fruitlet season.

In the validation of machine vision sensors for apple counting, the YOLOv9 Gelan-e configuration demonstrated superior accuracy across different sensor platforms. Notably, when utilizing Microsoft Azure sensors for counting Golden Delicious apples, YOLOv9 Gelan-e achieved the lowest RMSE of 6.29 and MAE of 5.19, outperforming other models. Similarly, for Scifresh apples captured using Intel Realsense cameras, YOLOv9 Gelan-e again led the performance metrics with an RMSE of 3.11 and an MAE of 2.46, marking the highest accuracy in counting validation among the tested configurations. Figures 11 and 12 depict the distributions of RMSE and MAE for the detection and counting of green apples across four varieties (Scilate, Scifresh, Honeycrisp, Cosmic Crisp) captured with an Apple iPhone 14, and two varieties (Golden Delicious and Scifresh) imaged using Microsoft Azure Kinect DK and Intel Realsense machine vision cameras.

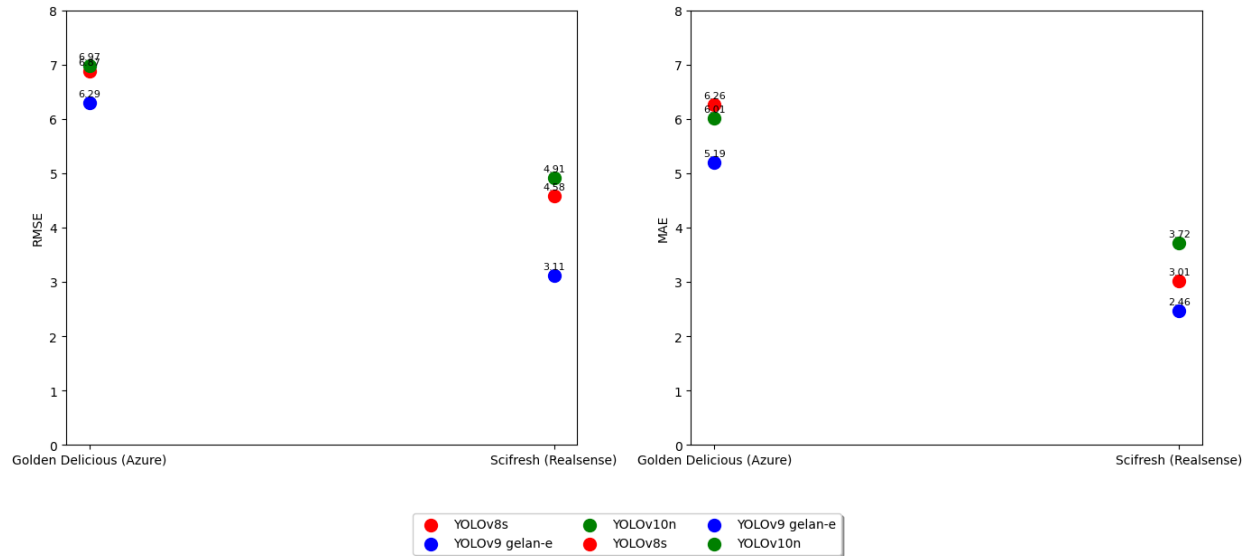


Figure 12: RMSE and MAE for Green Apple Detection Using Machine Vision Sensors Displays RMSE (left) and MAE (right) for green apple detection across YOLOv8s, YOLOv9 gelan-e, and YOLOv10n, assessed with Microsoft Azure and Intel Realsense sensors

For the IntelRealsense captured images in-field counting validation, YOLOv9 Gelan-e model achieved an RMSE of 2.46, significantly outperforming the best configurations of YOLOv8s and YOLOv10-N, which recorded RMSEs of 3.01 and 3.72, respectively. This notable discrepancy in performance underscores the impact of sensor-specific training on model efficacy. Models trained on a homogeneous dataset, such as those from a single type of sensor, are likely to exhibit enhanced performance when evaluated using data from the same source but may not generalize as well across data captured by different sensor technologies. The testing on a variety of apple types and through different sensors, including iPhone smartphones and Microsoft Azure machine vision sensors, further highlights this point. While the YOLOv9 Gelan-e model shows commendable results on Realsense data, the variation in performance across other sensors emphasizes the challenges in deploying machine vision systems that maintain high accuracy across diverse operational environments.

Figure 13 (a-f) showcases the adeptness of the leading YOLO configurations YOLOv8s, YOLOv9 Gelan-e, and YOLOv10n in detecting green apples within diverse orchard settings, as captured on an Apple iPhone. Specifically, subfigures 13a, 13b, and 13c highlight the detection capabilities of YOLOv8s, YOLOv9 Gelan-e, and YOLOv10n respectively on the Scilate apple variety. The subsequent subfigures 13d, 13e, and 13f replicate this analysis for the Scifresh variety, illustrating the consistent performance across different environmental conditions. These sections effectively demonstrate the specialized ability of YOLOv8s, YOLOv9 Gelan-e, and YOLOv10n to adapt to varying architectural and orchard scenarios, confirming their robustness and versatility in practical agricultural applications.

Figure 14 presents the detection and counting outcomes for Honeycrisp and Cosmic Crisp apple varieties, highlighting the performance of top YOLO configurations. Subfigures 14a and 14b illustrate that YOLOv8n and YOLOv9 Gelan-c accurately detected 5 out of 7 apples in a Honeycrisp cluster, demonstrating their effective recognition capabilities. However, YOLOv10n in subfigure 14c misidentified a background element as fruitlet, indicating a potential area for model refinement. For Cosmic Crisp apples, subfigures 14d and 14e show that both YOLOv8s and YOLOv9 Gelan-e successfully detected apples at the periphery, illustrating robust edge detection by these models. Conversely, YOLOv10 in subfigure 14f failed to recognize an apple in the annotated region, underscoring a detection limitation in this configuration. Additionally, YOLOv8s and YOLOv10n in subfigures 14d and 14f respectively, accurately

identified a green apple in the designated rectangular red encircled area, whereas YOLOv9 Gelan-e in subfigure 14c did not detect the apple, highlighting variability in performance across different models and scenarios.

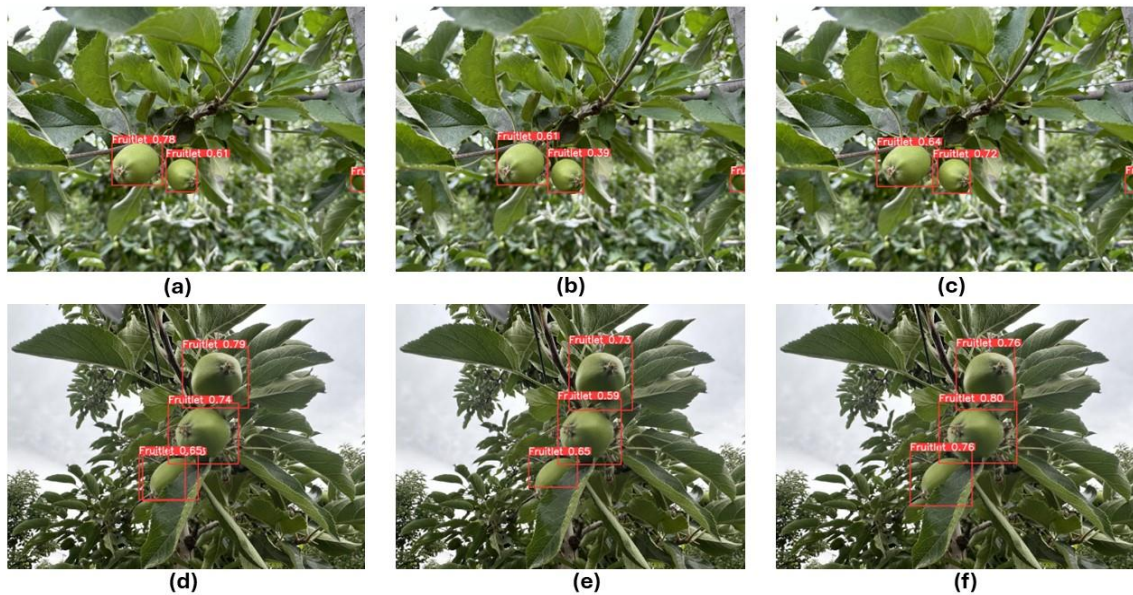


Figure 13: Performance of best YOLO configuration across YOLOv8, YOLOv9 and YOLOv10 Models in fruitlet detection on images collected by Apple Iphone on: 14 a) YOLOv8s on Scilate; b) YOLOv9 Gelan-e on Scilate; c) YOLOv10n on Scilate; d) YOLOv8s on Scifresh; e) YOLOv9 gelan-e on Scifresh; f) YOLOv10n on Scifresh

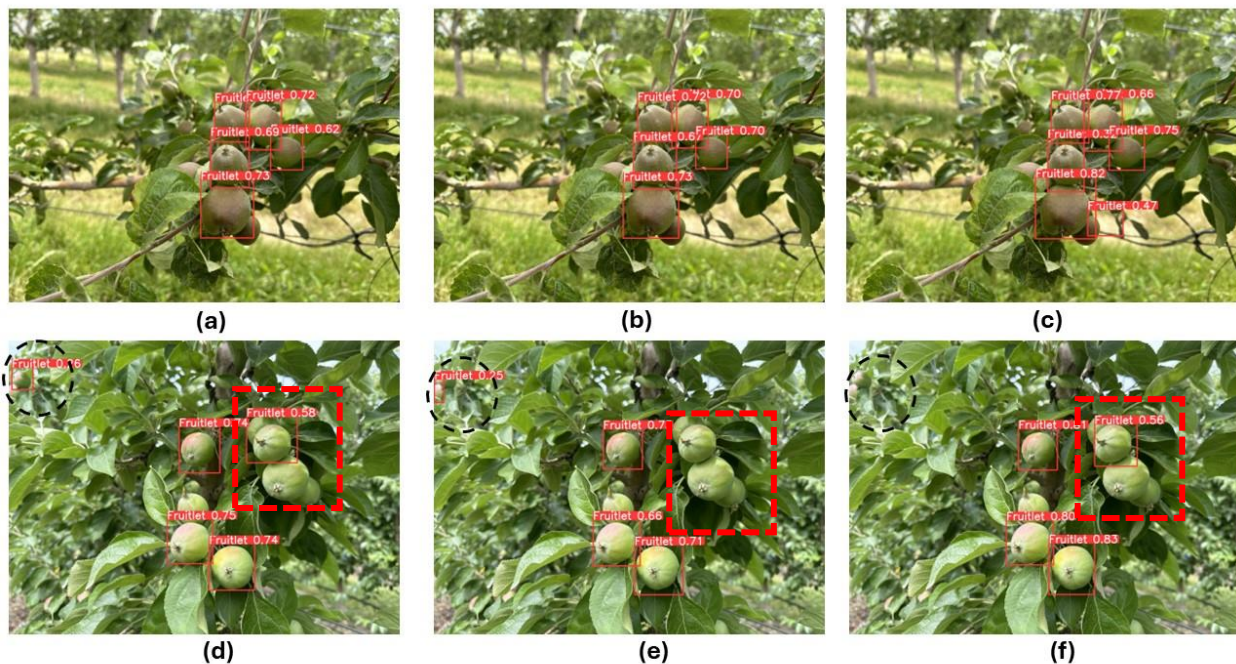


Figure 14: Performance of best YOLO configuration across YOLOv8, YOLOv9 and YOLOv10 Models in fruitlet detection on images collected by Apple Iphone on: a) YOLOv8n on Honeycrisp; b) YOLOv9 gelan-c on Honeycrisp; c) YOLOv10n misidentifies background on Honeycrisp; d) YOLOv8s detects edge apples on Cosmic Crisp; e) YOLOv9 gelan-e on Cosmic Crisp; f) YOLOv10 misses apple on Cosmic Crisp

Although the YOLO models demonstrated strong performance in detecting green apples from clusters in commercial orchards across four varieties, as shown in Figures 13 and 14, it is important to note the imaging context. The images were captured using an Apple iPhone 14, which offers high-contrast imaging with enhanced focus and resolution. In contrast, the deep learning models for YOLOv8, YOLOv9, and YOLOv10 were trained on RGB images acquired by IntelRealsense cameras, which differ in resolution, saturation, and overall image quality. This discrepancy highlights the robustness of the models, as they were never trained on the specific varieties shown or on images from the iPhone camera. Despite these differences, the exemplary performance of configurations like YOLOv9 Gelan-e, YOLOv8s, and YOLOv10n showcases their potential for fruitlet detection. This study, involving 1,149 images, suggests that expanding the training datasets and employing more computationally intense environments could further enhance model accuracy and generalizability.

Figure 15 illustrates the validation performance of the best-configured models from the YOLO series YOLOv8s, YOLOv9 Gelan-e, and YOLOv10n across two distinct apple varieties and sensing technologies. Subfigures 15a, 15b, and 15c display the detection outcomes for the Golden Delicious variety using the Microsoft Azure Kinect DK machine vision sensor. Notably, in the dark circle-dotted regions of Figure 15a, YOLOv8s failed to detect two camouflaged green apples, whereas YOLOv9 Gelan-e successfully identified these apples in Figure 15b. YOLOv10n, while detecting one of the two apples, exhibited a partial performance in Figure 15c. In contrast, subfigures 15d, 15e, and 15f present detection results from Intel Realsense D435i-captured RGB images within a Scifresh apple orchard. YOLOv8s showcased a robust detection capability in Figure 15d, effectively identifying almost all apples within the frame, including those in a challenging yellow encircled dotted region where the fruits were obscured by leaves and stems. Similarly, both YOLOv9 Gelan-e and YOLOv10n demonstrated high accuracy in discerning the occluded green apples in Figures 15e and 15f, respectively.

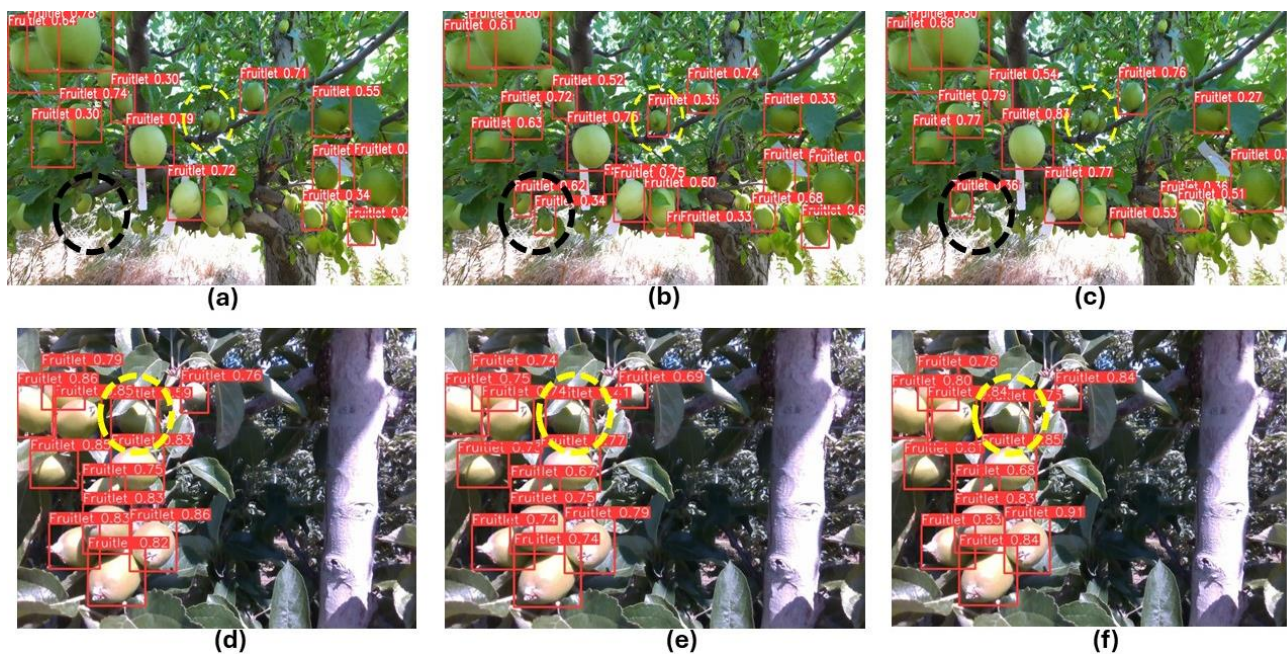


Figure 15: Validation of Optimal YOLO Configurations on Different Apple Varieties and Sensors a) YOLOv8s detection on Golden Delicious using Microsoft Azure Kinect DK, missing camouflaged apples; b) YOLOv9 gelan-e detects camouflaged apples on Golden Delicious; c) YOLOv10n detects one of two camouflaged apples on Golden Delicious; d) YOLOv8s accurately identifies apples in a Scifresh orchard captured with IntelRealsense, despite occlusions; e) YOLOv9 gelan-e identifies occluded apples in Scifresh orchard; f) YOLOv10n also detects occluded apples in Scifresh orchard, demonstrating high accuracy

5. Conclusion and Future Suggestions

In this study, we conducted a comprehensive evaluation of various configurations of three state-of-the-art YOLO object detection models (YOLOv8, YOLOv9, and YOLOv10) to assess their effectiveness in detecting green apples before thinning in complex orchard environments using different sensors and conditions. The specific conclusions and future suggestions of this study are specifically summarized in following five points:

- **Model-Specific Performance:** YOLOv10n configuration demonstrated exceptional efficiency in postprocessing with a remarkable speed of 1.6 ms. On the other hand, YOLOv8n showed superior inference capabilities, processing images in just 4.1 ms, indicative of its robust object recognition. Meanwhile, YOLOv8x led in preprocessing speed, readying images for detection at a swift rate of 0.9 ms.
- **Accuracy Across Configurations:** YOLOv9 models, particularly YOLOv9 Gelan-e and YOLOv9 base, achieved the highest mean Average Precision at 50% Intersection over Union (mAP@0.50) scores, highlighting their superior accuracy in object detection. YOLOv9 configurations also showed excellent precision and recall, with YOLOv9 Gelan-c reaching a high precision of 0.903 and YOLOv9 Gelan-m achieving the best recall at 0.899.
- **Counting Validation:** The YOLOv9 Gelan-e model excelled in counting validation across different sensors and apple varieties. It performed exceptionally well in tests conducted using Intel Realsense cameras, leading to the lowest RMSE and MAE scores, which were significantly better than those achieved by other configurations.
- **Sensor-Specific Training Impact:** The study demonstrated that training models on data collected from a specific type of sensor, such as Intel Realsense, significantly enhances model performance when tested with data from the same sensor. This indicates the importance of including diverse sensor data in training phases to ensure robust model performance across various deployment scenarios.
- **Recommendations for Model Deployment:** Given the varying performance across different models and sensor types, deploying YOLO models in practical applications requires careful consideration of the specific model configuration and the sensor data used for training. For tasks requiring high accuracy and speed, YOLOv9 Gelan-e, particularly when trained with matching sensor data, is recommended due to its superior detection capabilities.

Acknowledgements and Funding

This work was supported by the National Science Foundation and United States Department of Agriculture, National Institute of Food and Agriculture through the “Artificial Intelligence (AI) Institute for Agriculture” Program under Award AWD003473, Zhejiang Provincial Natural Science Foundation (Grant No. LD24E050006, LGN22C130006), and the National Natural Science Foundation of China (Grant No. 32372004).

The authors express their heartfelt gratitude to Dave Allan from Allan Brothers Apple Company, which is one of the largest commercial apples growing company over North America, for granting access to the commercial orchard, facilitating this research. Special thanks are also due to Christine Cromar, Bonnie Copeland, Patrick Scharf, Achyut Paudel and Priyanka Upadhayay for their essential support in logistics.

References

- [1] M. Mhamed, Z. Zhang, J. Yu, Y. Li, and M. Zhang, “Advances in apple’s automated orchard equipment: A comprehensive research,” *Comput Electron Agric*, vol. 221, p. 108926, 2024.
- [2] F. Xiao, H. Wang, Y. Xu, and R. Zhang, “Fruit detection and recognition based on deep learning for automatic harvesting: an overview and review,” *Agronomy*, vol. 13, no. 6, p. 1625, 2023.
- [3] Q. Zhang, M. Karkee, and A. Tabb, “The use of agricultural robots in orchard management,” in *Robotics and automation for improving agriculture*, Burleigh Dodds Science Publishing, 2019, pp. 187–214.
- [4] R. Sapkota, D. Ahmed, M. Churuvija, and M. Karkee, “Immature Green Apple Detection and Sizing in Commercial Orchards using YOLOv8 and Shape Fitting Techniques,” *IEEE Access*, vol. 12, pp. 43436–43452, 2024.
- [5] R. Sapkota, D. Ahmed, and M. Karkee, “Comparing YOLOv8 and Mask R-CNN for instance segmentation in complex orchard environments,” *Artificial Intelligence in Agriculture*, 2024, doi: <https://doi.org/10.1016/j.aiaa.2024.07.001>.
- [6] F. G. J. Dennis, “The history of fruit thinning,” *Plant Growth Regul*, vol. 31, pp. 1–16, 2000.
- [7] F. G. J. Dennis, “The history of fruit thinning,” *Plant Growth Regul*, vol. 31, pp. 1–16, 2000.
- [8] G. Costa, A. Botton, and G. Vizzotto, “Fruit thinning: Advances and trends,” *Hortic. Rev*, vol. 46, pp. 185–226, 2018.
- [9] M. Wei, H. Wang, T. Ma, Q. Ge, Y. Fang, and X. Sun, “Comprehensive utilization of thinned unripe fruits from horticultural crops,” *Foods*, vol. 10, no. 9, p. 2043, 2021.
- [10] USApple, “The Voice of the Apple Industry,” 2021.
- [11] UCDAVIS Gifford Center for Population Studies, “Farm Labor in the 2020s Demand, Supply, and Markets - Report,” <https://afop.org/cif/learn-the-facts/>.
- [12] D. Ahmed, R. Sapkota, M. Churuvija, and M. Karkee, “Machine vision-based crop-load estimation using yolov8,” *arXiv preprint arXiv:2304.13282*, 2023.

- [13] D. Bochtis, L. Benos, M. Lampridi, V. Marinoudi, S. Pearson, and C. G. Sørensen, “Agricultural workforce crisis in light of the COVID-19 pandemic,” *Sustainability*, vol. 12, no. 19, p. 8212, 2020.
- [14] J. L. Lusk and R. Chandra, “Farmer and farm worker illnesses and deaths from COVID-19 and impacts on agricultural output,” *PLoS One*, vol. 16, no. 4, p. e0250621, 2021.
- [15] United Nations, “World Urbanization Prospects,” The 2018 Revision.
- [16] USDA, “Share of hired farm labor cost to total cash expenses, 2018,” 2018.
- [17] V. Marinoudi, C. G. Sørensen, S. Pearson, and D. Bochtis, “Robotics and labour in agriculture. A context consideration,” *Biosyst Eng*, vol. 184, pp. 111–121, 2019.
- [18] J. J. May and T. A. Arcury, “Occupational injury and illness in farmworkers in the eastern United States,” *Latinx Farmworkers in the Eastern United States: Health, Safety, and Justice*, pp. 41–81, 2020.
- [19] G. Earle-Richardson, P. L. Jenkins, D. Strogatz, E. M. Bell, and J. J. May, “Development and initial assessment of objective fatigue measures for apple harvest work,” *Appl Ergon*, vol. 37, no. 6, pp. 719–727, 2006.
- [20] T. KATAOKA, H. Okamoto, and S. Hata, “Automatic detecting system of apple harvest season for robotic apple harvesting,” in *2001 ASAE Annual Meeting*, American Society of Agricultural and Biological Engineers, 1998, p. 1.
- [21] J. Zhao, J. Tow, and J. Katupitiya, “On-tree fruit recognition using texture properties and color data,” in *2005 IEEE/RSJ International Conference on Intelligent Robots and Systems*, IEEE, 2005, pp. 263–268.
- [22] T. T. Nguyen, K. Vandevoorde, E. Kayacan, J. de Baerdemaeker, and W. Saeys, “Apple detection algorithm for robotic harvesting using a RGB-D camera,” in *International Conference of Agricultural Engineering, Zurich, Switzerland*, 2014.
- [23] J. Wachs, H. I. Stern, T. Burks, V. Alchanatis, and I. Bet-Dagan, “Apple detection in natural tree canopies from multimodal images,” in *Proceedings of the 7th European Conference on Precision Agriculture, Wageningen, The Netherlands*, 2009, p. 293302.
- [24] J. P. Wachs, H. I. Stern, T. Burks, and V. Alchanatis, “Low and high-level visual feature-based apple detection from multi-modal images,” *Precis Agric*, vol. 11, pp. 717–735, 2010.

- [25] G. Xuan *et al.*, “Apple detection in natural environment using deep learning algorithms,” *IEEE Access*, vol. 8, pp. 216772–216780, 2020.
- [26] K. G. Liakos, P. Busato, D. Moshou, S. Pearson, and D. Bochtis, “Machine learning in agriculture: A review,” *Sensors*, vol. 18, no. 8, p. 2674, 2018.
- [27] A. Kuznetsova, T. Maleva, and V. Soloviev, “Using YOLOv3 algorithm with pre-and post-processing for apple detection in fruit-harvesting robot,” *Agronomy*, vol. 10, no. 7, p. 1016, 2020.
- [28] S. Puttemans, Y. Vanbrabant, L. Tits, and T. Goedemé, “Automated visual fruit detection for harvest estimation and robotic harvesting,” in *2016 sixth international conference on image processing theory, tools and applications (IPTA)*, IEEE, 2016, pp. 1–6.
- [29] G. Xuan *et al.*, “Apple detection in natural environment using deep learning algorithms,” *IEEE Access*, vol. 8, pp. 216772–216780, 2020.
- [30] H. Kang and C. Chen, “Fast implementation of real-time fruit detection in apple orchards using deep learning,” *Comput Electron Agric*, vol. 168, p. 105108, 2020.
- [31] S. Sun, M. Jiang, D. He, Y. Long, and H. Song, “Recognition of green apples in an orchard environment by combining the GrabCut model and Ncut algorithm,” *Biosyst Eng*, vol. 187, pp. 201–213, 2019.
- [32] R. Linker, O. Cohen, and A. Naor, “Determination of the number of green apples in RGB images recorded in orchards,” *Comput Electron Agric*, vol. 81, pp. 45–57, 2012.
- [33] X. Xia *et al.*, “Detection of young green apples for fruit robot in natural scene.,” *Journal of Agricultural Science and Technology (Beijing)*, vol. 20, no. 5, pp. 64–74, 2018.
- [34] Y. Tian, G. Yang, Z. Wang, H. Wang, E. Li, and Z. Liang, “Apple detection during different growth stages in orchards using the improved YOLO-V3 model,” *Comput Electron Agric*, vol. 157, pp. 417–426, 2019.
- [35] Z. Huang, P. Zhang, R. Liu, and D. Li, “Immature apple detection method based on improved Yolov3,” *ASP Transactions on Internet of Things*, vol. 1, no. 1, pp. 9–13, 2021.
- [36] D. Wang and D. He, “Channel pruned YOLO V5s-based deep learning approach for rapid and accurate apple fruitlet detection before fruit thinning,” *Biosyst Eng*, vol. 210, pp. 271–281, 2021.

- [37] Z. Zheng *et al.*, “A method of green citrus detection in natural environments using a deep convolutional neural network,” *Front Plant Sci*, vol. 12, p. 705737, 2021.
- [38] J. Wang *et al.*, “PG-YOLO: An efficient detection algorithm for pomegranate before fruit thinning,” *Eng Appl Artif Intell*, vol. 134, p. 108700, 2024.
- [39] X. Fu *et al.*, “Green Fruit Detection with a Small Dataset under a Similar Color Background Based on the Improved YOLOv5-AT,” *Foods*, vol. 13, no. 7, p. 1060, 2024.
- [40] W. Jia *et al.*, “An accurate green fruits detection method based on optimized YOLOX-m,” *Front Plant Sci*, vol. 14, p. 1187734, 2023.
- [41] H. Sun, B. Wang, and J. Xue, “YOLO-P: An efficient method for pear fast detection in complex orchard picking environment,” *Front Plant Sci*, vol. 13, p. 1089454, 2023.
- [42] W. Yijing, Y. Yi, W. Xue-fen, C. Jian, and L. Xinyun, “Fig fruit recognition method based on YOLO v4 deep learning,” in *2021 18th International Conference on Electrical Engineering/Electronics, Computer, Telecommunications and Information Technology (ECTI-CON)*, IEEE, 2021, pp. 303–306.
- [43] F. Wang *et al.*, “A lightweight Yunnan Xiaomila detection and pose estimation based on improved YOLOv8,” *Front Plant Sci*, vol. 15, p. 1421381, 2024.
- [44] Y. Niu, M. Lu, X. Liang, Q. Wu, and J. Mu, “YOLO-plum: A high precision and real-time improved algorithm for plum recognition,” *PLoS One*, vol. 18, no. 7, p. e0287778, 2023.
- [45] R. Tang, Y. Lei, B. Luo, J. Zhang, and J. Mu, “YOLOv7-Plum: advancing plum fruit detection in natural environments with deep learning,” *Plants*, vol. 12, no. 15, p. 2883, 2023.
- [46] W. Chen, S. Lu, B. Liu, M. Chen, G. Li, and T. Qian, “CitrusYOLO: a algorithm for citrus detection under orchard environment based on YOLOV4,” *Multimed Tools Appl*, vol. 81, no. 22, pp. 31363–31389, 2022.
- [47] H. Mirhaji, M. Soleymani, A. Asakereh, and S. A. Mehdizadeh, “Fruit detection and load estimation of an orange orchard using the YOLO models through simple approaches in different imaging and illumination conditions,” *Comput Electron Agric*, vol. 191, p. 106533, 2021.
- [48] J. Wang, Z. Gao, Y. Zhang, J. Zhou, J. Wu, and P. Li, “Real-time detection and location of potted flowers based on a ZED camera and a YOLO V4-tiny deep learning algorithm,” *Horticulturae*, vol. 8, no. 1, p. 21, 2021.

- [49] D. Wu, S. Lv, M. Jiang, and H. Song, "Using channel pruning-based YOLO v4 deep learning algorithm for the real-time and accurate detection of apple flowers in natural environments," *Comput Electron Agric*, vol. 178, p. 105742, 2020.
- [50] S. R. Khanal, R. Sapkota, D. Ahmed, U. Bhattarai, and M. Karkee, "Machine Vision System for Early-stage Apple Flowers and Flower Clusters Detection for Precision Thinning and Pollination," *IFAC-PapersOnLine*, vol. 56, no. 2, pp. 8914–8919, 2023.
- [51] M. H. Junos, A. S. Mohd Khairuddin, S. Thannirmalai, and M. Dahari, "An optimized YOLO-based object detection model for crop harvesting system," *IET Image Process*, vol. 15, no. 9, pp. 2112–2125, 2021.
- [52] W. Yijing, Y. Yi, W. Xue-fen, C. Jian, and L. Xinyun, "Fig fruit recognition method based on YOLO v4 deep learning," in *2021 18th International Conference on Electrical Engineering/Electronics, Computer, Telecommunications and Information Technology (ECTI-CON)*, IEEE, 2021, pp. 303–306.
- [53] F. Xiao, H. Wang, Y. Xu, and R. Zhang, "Fruit detection and recognition based on deep learning for automatic harvesting: an overview and review," *Agronomy*, vol. 13, no. 6, p. 1625, 2023.
- [54] Y. Zhang, L. Li, C. Chun, Y. Wen, and G. Xu, "Multi-scale feature adaptive fusion model for real-time detection in complex citrus orchard environments," *Comput Electron Agric*, vol. 219, p. 108836, 2024.
- [55] J. Redmon, S. Divvala, R. Girshick, and A. Farhadi, "You only look once: Unified, real-time object detection," in *Proceedings of the IEEE conference on computer vision and pattern recognition*, 2016, pp. 779–788.
- [56] C. M. Badgujar, A. Poulouse, and H. Gan, "Agricultural object detection with You Only Look Once (YOLO) Algorithm: A bibliometric and systematic literature review," *Comput Electron Agric*, vol. 223, p. 109090, 2024.
- [57] M. G. Ragab et al., "A Comprehensive Systematic Review of YOLO for Medical Object Detection (2018 to 2023)," *IEEE Access*, 2024.
- [58] N. M. A. A. Dazlee, S. A. Khalil, S. Abdul-Rahman, and S. Mutalib, "Object detection for autonomous vehicles with sensor-based technology using yolo," *International Journal of Intelligent Systems and Applications in Engineering*, vol. 10, no. 1, pp. 129–134, 2022.
- [59] A. Vijayakumar and S. Vairavasundaram, "Yolo-based object detection models: A review and its applications," *Multimed Tools Appl*, pp. 1–40, 2024.

- [60] M. Hussain, “YOLO-v1 to YOLO-v8, the rise of YOLO and its complementary nature toward digital manufacturing and industrial defect detection,” *Machines*, vol. 11, no. 7, p. 677, 2023.
- [61] H. Nakahara, H. Yonekawa, T. Fujii, and S. Sato, “A lightweight YOLOv2: A binarized CNN with a parallel support vector regression for an FPGA,” in *Proceedings of the 2018 ACM/SIGDA International Symposium on field-programmable gate arrays*, 2018, pp. 31–40.
- [62] R. Li and J. Yang, “Improved YOLOv2 object detection model,” in *2018 6th international conference on multimedia computing and systems (ICMCS)*, IEEE, 2018, pp. 1–6.
- [63] K.-J. Kim, P.-K. Kim, Y.-S. Chung, and D.-H. Choi, “Performance enhancement of YOLOv3 by adding prediction layers with spatial pyramid pooling for vehicle detection,” in *2018 15th IEEE international conference on advanced video and signal based surveillance (AVSS)*, IEEE, 2018, pp. 1–6.
- [64] U. Nepal and H. Eslamiat, “Comparing YOLOv3, YOLOv4 and YOLOv5 for autonomous landing spot detection in faulty UAVs,” *Sensors*, vol. 22, no. 2, p. 464, 2022.
- [65] N. Mohod, P. Agrawal, and V. Madaan, “YOLOv4 vs YOLOv5: Object detection on surveillance videos,” in *International Conference on Advanced Network Technologies and Intelligent Computing*, Springer, 2022, pp. 654–665.
- [66] C. Li et al., “YOLOv6: A single-stage object detection framework for industrial applications,” *arXiv preprint arXiv:2209.02976*, 2022.
- [67] R. Sapkota et al., “YOLOv10 to Its Genesis: A Decadal and Comprehensive Review of The You Only Look Once Series,” *arXiv preprint arXiv:2406.19407*, 2024.
- [68] C.-Y. Wang, I.-H. Yeh, and H.-Y. M. Liao, “YOLOv9: Learning What You Want to Learn Using Programmable Gradient Information,” *arXiv preprint arXiv:2402.13616*, 2024.
- [69] A. Wang et al., “Yolov10: Real-time end-to-end object detection,” *arXiv preprint arXiv:2405.14458*, 2024.